symmetry

MDPI

Article

An ONIOM-Based High-Level Thermochemistry Study on Hydrogen Abstraction Reactions of Large Straight-Chain Alkanes by Hydrogen, Hydroxyl, and Hydroperoxyl Radicals

Yicheng Chi [1,2], Hao Pan [1,*], Qinghui Meng [3], Lidong Zhang [3] and Peng Zhang [2]

[1] School of Automotive and Transportation Engineering, Shenzhen Polytechnic University, Shenzhen 518005, China
[2] Department of Mechanical Engineering, City University of Hong Kong, Kowloon Tong 999077, Hong Kong; penzhang@cityu.edu.hk
[3] National Laboratory of Synchrotron, University of Science and Technology of China, Hefei 230029, China; meng0260@umn.edu (Q.M.); zld@ustc.edu.cn (L.Z.)
* Correspondence: panhao@szpu.edu.cn

Abstract: Accurate thermochemical data are of great importance in developing quantitatively predictive reaction mechanisms for transportation fuels, such as diesel and jet fuels, which are primarily composed of large hydrocarbon molecules, especially large straight-chain alkanes containing more than 10 carbon atoms. This paper presents an ONIOM[QCISD(T)/CBS:DFT]-based theoretical thermochemistry study on the hydrogen abstraction reactions of straight-chain alkanes, n-C_nH_{2n+2}, (n = 1–16) by hydrogen (H), hydroxyl (OH), and hydroperoxyl (HO_2) radicals. These reactions, with $n \geq 10$, pose significant computational challenges for prevalent high-level ab initio methods. However, they are effectively addressed using the ONIOM-based method. One notable aspect of this study is the consideration of the high symmetry of straight-chain alkanes. This symmetry allows us to study half of the reactions, employing a generalized approach. Therefore, a total of 216 reactions are systematically studied for the three reaction systems. Our results align very well with those from the widely accepted high-level QCISD(T)/CBS method, with discrepancies between the two generally less than 0.10 kcal/mol. Furthermore, we compared large straight-chain alkanes (n-$C_{16}H_{34}$ and n-$C_{18}H_{38}$) with large methyl ester molecules ($C_{15}H_{31}COOCH_3$ and $C_{17}H_{33}COOCH_3$) to elucidate the impact of functional groups (ester group and C=C double bond) on the reactivity of the long-chain structure. These findings underscore the accuracy and efficiency of the ONIOM-based method in computational thermochemistry, particularly for large straight-chain hydrocarbons in transportation fuels.

Keywords: large straight-chain alkanes; hydrogen abstraction reaction; energy barrier; heat of reaction; ONIOM

Citation: Chi, Y.; Pan, H.; Meng, Q.; Zhang, L.; Zhang, P. An ONIOM-Based High-Level Thermochemistry Study on Hydrogen Abstraction Reactions of Large Straight-Chain Alkanes by Hydrogen, Hydroxyl, and Hydroperoxyl Radicals. *Symmetry* **2024**, *16*, 367. https://doi.org/10.3390/sym16030367

Academic Editor: Anthony Harriman

Received: 22 February 2024
Revised: 12 March 2024
Accepted: 12 March 2024
Published: 18 March 2024

1. Introduction

The contemporary concern for energy safety and environmental protection has spurred lasting studies on developing advanced combustion energy conversion devices. The aim of investigating fuel combustion chemistry is to understand and analyze the combustion processes for enhancing combustion efficiency, controlling combustion stability, and reducing combustion emissions [1]. The increasing demand for carbon neutralization necessitates comprehensive and systematic research on petroleum-based fuels to make rational use of them.

There is a well-recognized difficulty in studying the combustion chemistry (including thermochemistry and chemical kinetics) of practical fuels such as gasoline, diesel, and jet fuels, due to their complex composition. These fuels generally consist of hundreds of hydrocarbon molecules, with n-alkanes being one of the primary components [2–7]. To mitigate this difficulty, a widely accepted strategy involves using surrogate fuels. These

surrogate fuels are composed of several key components that effectively represent the characteristics of practical fuels. Many previous studies have indicated that large hydrocarbon molecules, containing more than 10 carbon atoms, are often primary components in these surrogate fuels [2,6,7].

For gasoline fuels, Mehl et al. [8] developed linear and branched saturated hydrocarbons (*iso*-octane and *n*-heptane), olefins (1-hexene), and aromatics (toluene) as the gasoline surrogates for kinetic modelling. Jerzembeck et al. [9] and Sileghem et al. [10] demonstrated that the laminar burning velocities of two-component (*n*-heptane and *iso*-octane) and three-component gasoline surrogates (*iso*-octane, *n*-heptane, and toluene) corresponded well with those of commercial gasoline.

For diesel fuels, Lemaire et al. [11] adopted two diesel surrogates to study soot formation in turbulent flames compared with commercial diesel. The first surrogate consisted of 70% *n*-decane and 30% α-methylnaphthalene by moles, and the second comprised 80% *n*-decane and 20% α-methylnaphthalene by moles. Mati et al. [12] used a five-component surrogate to represent diesel fuel, consisting of 36.1% *n*-hexadecane, 23.1% *n*-propylcyclohexane, 18.7% *n*-propylbenzene, 14.7% *iso*-octane, and 7.4% 1-methylnaphthalene, all percentages by weight.

For jet fuels, Honnet et al. [13] developed the Aachen surrogate to represent JP-8, consisting of 80% *n*-decane and 20% 1,2,4-trimethylbenzene by weight. Dagaut et al. [14] used a 1- to 3-component surrogate model fuel to represent Jet-A1, which includes various combinations: 100% *n*-decane; a mix of 74% *n*-decane and 26% *n*-propylbenzene by mole; a combination of 74% *n*-decane and 26% *n*-propylcyclohexane by mole; and a blend of 74% *n*-decane, 15% *n*-propylbenzene, and 11% *n*-propylcyclohexane by mole. Strelkova et al. [15] adopted a Jet-A surrogate mixture, comprising 72.7% *n*-decane, 9.1% *n*-hexane, and 18.2% benzene by weight. Mawid et al. [16] proposed three multicomponent surrogates for JP-8, primarily containing large straight-chain alkanes such as *n*-decane, *n*-dodecane, *n*-tetradecane, and *n*-hexadecane. Dahm et al. [17] also conducted an experimental and modelling study on the pyrolysis of n-dodecane, as it is an important component of some jet fuels.

In light of the fact that large straight-chain alkanes are the main components of surrogate fuels representing various practical fuels, and considering their significant impact on ignition delay, laminar flame speed, heat release, soot formation, etc., extensive studies have focused on developing chemical kinetics modeling for these surrogate fuels [2,18–20]. The development of a typically detailed reaction mechanism for a large straight-chain alkane is a formidable task, involving hundreds of species and thousands of elementary reactions. Specifying thermochemical and kinetic data for such a vast number of species and reactions presents significant challenges. Due to the lack of sufficient theoretical and experimental studies for large hydrocarbon species, the existing detailed mechanisms for these species [21–23] have relied on thermodynamic data obtained using the THERM program [24,25], which employs the group additivity rules of Benson [26].

Recent advances in electronic structure theory have enabled us to obtain thermochemical data for relatively small molecules that are comparable to those from well-conducted experiments. For example, the uncertainties of CCSD(T)/CBS (the coupled cluster theory with single and double excitations and a quasiperturbative treatment of connected triple excitations, extrapolated to a complete basis set) are usually less than 1.1 kcal/mol [27] for the predictions of barrier height and reaction energy. QCISD(T)/CBS (the quadratic configuration interaction with singles, doubles, and a perturbative inclusion of triples, also extrapolated to complete basis sets) typically yields predictions with uncertainties around 1.0 kcal/mol [28]. This accuracy can be further improved to 0.6 kcal/mol [29] by including a bond additivity correction. However, these high-level methods are not feasible for systems with more than 10 nonhydrogen atoms, given the common computational capacity of supercomputers. As a result, most reaction systems have been studied at lower levels, such as CBS-QB3 [30] and B3LYP/6-31G(d,p) [31], due to computational constraints.

Zhang and Zhang [32] proposed a two-layer ONIOM (our own N-layered integrated molecular orbital and molecular mechanics) method [33]. In this method, the QCISD(T)/CBS approach is employed for the high layer, while the B3LYP-favored density functional theory (DFT) method is used for the low layer. The ONIOM [QCISD(T)/CBS:DFT] method was systematically validated in studies of hydrogen abstraction reaction systems involving saturated and unsaturated alkyl esters with a hydrogen atom [32,34]. The calculated energies showed very good agreement with those obtained using the QCISD(T)/CBS method alone. This was verified by the discrepancies being generally less than 0.15 kcal/mol in almost all the test cases.

Among the key reactions relevant to combustion are the hydrogen abstraction reactions of these straight-chain alkanes by the hydrogen (H), hydroxyl (OH), and hydroperoxyl (HO_2) radicals [35–39]. To date, direct experimental measurements for these reactions ($n > 4$) have been scarce, with few critical studies addressing the reactions of these radicals with large alkanes [40–42]. Specifically, the hydrogen abstraction reactions from *n*-alkane by the HO_2 radical constitute an important class of reactions in low-to-mid temperature combustion chemistry, playing a crucial role in ignition. However, experimentally measuring the reaction rate constants of these elementary reactions is challenging. On the one hand, these reactions have high energy barriers, greater than 10 kcal/mol, resulting in lower rate constants. On the other hand, increasing the temperature to raise the rate constants leads to the decomposition of HO_2 radicals. Consequently, there are only a few sets of experimental data [43–46] for the reactions of *n*-alkane with HO_2 radical. These data were obtained using indirect measurement techniques and are applicable only within a narrow temperature range. Therefore, data obtained from the theoretical high-level methods are important to the high-level chemical kinetic calculation.

Regarding the use of high-level ab initio chemical kinetics for hydrocarbon molecules, most previous studies have primarily focused on relatively small hydrocarbon molecules [37,42,47–52]. This focus is mainly because the prevalent high-level methods based on electronic structure theory are computationally demanding for large hydrocarbon molecules. Wu et al. [53] and Chi et al. [54] proposed the variant MS-T methods and systematically validated these methods for the straight-chain alkanes. However, it is important to note that these methods have not been applied to larger systems.

It should be noted that, for the larger system, Meng et al. [55] employed high-level orbital-based and ONIOM-based methods to closely examine the Bell–Evans–Polanyi (BEP) correlations for hydrogen abstraction reactions of biodiesel surrogates (methyl decanoate) by H and OH radicals, achieving deviations of less than 0.90 kcal/mol. Furthermore, Sarathy et al. [56] established a detailed skeletal mechanism consisting of 648 species and 2998 reactions for biodiesel (methyl decanoate). It is important to note that the thermochemical data, such as energy barriers, were not obtained through high-level calculations. The group additivity (GA) and BEP correlations, representing an empirical relationship with system-dependent coefficients, inherently limit their predictive capacity across diverse chemical systems. This limitation is particularly evident when considering the transition from small to large molecular structures, such as the hydrogen abstraction reactions of *n*-C_nH_{2n+2}, (n = 1–16) by hydrogen (H), hydroxyl (OH), and hydroperoxyl (HO_2) radicals, as investigated in our study. Therefore, the results calculated using high-level methods offer a valuable opportunity to refine and improve the accuracy of the GA and BEP correlations for a broader range of chemical systems. Additionally, it should be mentioned that the present study primarily focuses on the enthalpic contributions to the thermochemistry of large straight-chain alkanes. Although hindered rotations (HRs) play a crucial role in the thermochemical properties of compounds, their effects are predominantly observed in the entropy component of the Gibbs free energy, rather than directly influencing enthalpy.

In light of our findings, we have identified a notable gap in the availability of comprehensive thermochemical and kinetic data for large straight-chain alkanes, particularly when examined using advanced theoretical methods. Addressing this gap, the present study systematically investigates the hydrogen abstraction reactions of extensive straight-chain

alkanes, specifically, *n*-C_nH_{2n+2} (n = 1–16), by H, OH, and HO_2 radicals using the high-level ONIOM[QCISD(T)/CBS:DFT] method [32]. A unique aspect of the study is the thorough examination of all potential hydrogen abstraction sites across diverse reaction types in each system. This includes an in-depth analysis of 216 distinct reactions, categorized into three sets: 72 involving *n*-C_nH_{2n+2} + H (denoted by H-R1 to H-R72), another 72 with C_nH_{2n+2} + OH (denoted by OH-R1 to OH-R72), and 72 more with *n*-C_nH_{2n+2} + HO_2 (denoted by HO_2-R1 to HO_2-R72). The novelty of this study lies in its comprehensive scope and the application of high-level computational techniques to large hydrocarbons, a challenging endeavor rarely undertaken in previous studies. Moreover, the present study not only demonstrates the versatility and efficacy of the ONIOM method for complex hydrocarbon analysis but also contributes significantly to the field by providing essential benchmark data for the thermochemistry of these large molecular systems.

2. Computational Methods

2.1. Potential Energy Surface

The geometries optimization and vibrational frequencies for all stationary points on the potential energy surfaces of these hydrogen abstraction reactions were conducted at the B3LYP/6-311++G(d,p) level [57] for both *n*-C_nH_{2n+2} + H and *n*-C_nH_{2n+2} + HO_2 (n = 1–16). For *n*-C_nH_{2n+2} + OH (n = 1–16), the calculations were performed at the M06-2X/6-311++G(d,p) level [58]. The identified transition states in these reactions were confirmed by intrinsic reaction coordinate (IRC) analysis to examine the connections of each saddle point to its respective local minima. Zero-point energy (ZPE) corrections were obtained at the same computational level as the reactions.

2.2. QCISD(T)/CBS and ONIOM Energies

2.2.1. QCISD(T)/CBS Single-Point Energies

In the present study, the computational load is determined by the number of nonhydrogen atoms (carbon and oxygen atoms) in the hydrogen abstraction reaction systems of *n*-C_nH_{2n+2} + H, OH, and HO_2 (n = 1–16). For relatively small molecules, two high-level ab initio methods were employed to produce benchmark data for validating the ONIOM method. The first method, $[QCISD(T)/CBS]_1$, is based on the direct extrapolation of energies using the correlation-consistent, polarized valence, cc-pVTZ, and cc-pVQZ basis sets of Dunning [59,60] to the complete basis set (CBS) limit [61] by

$$\begin{aligned} E[QCISD(T)/CBS]_1 &= E[QCISD(T)/CBS]_{TZ\rightarrow QZ} \\ &= E[QCISD(T)/QZ] + \{E[QCISD(T)/QZ] \\ &\quad -E[QCISD(T)/TZ]\} \times 0.6938 \end{aligned} \tag{1}$$

Equation (1) estimates the CBS limit energy using the QCISD(T) method by extrapolating from triple zeta (TZ) to quadruple zeta (QZ) basis sets. E[QCISD(T)/QZ] and E[QCISD(T)/TZ] are the energies calculated with QZ and TZ basis sets, respectively. The factor 0.6938 is a scaling constant used to refine the estimate.

However, when the number of nonhydrogen atoms in reactions exceeds 5, the computation cost of Equation (1) increases significantly. This is due to the dramatically increasing computation load required for cc-pVQZ calculations. Therefore, for these larger systems, we adopted an alternative method, $[QCISD(T)/CBS]_2$ [62], given by

$$\begin{aligned} E[QCISD(T)/CBS]_2 &= E[QCISD(T)/CBS]_{DZ\rightarrow TZ} + \{E[MP2/CBS]_{TZ\rightarrow QZ} \\ &\quad -E[MP2/CBS]_{DZ\rightarrow TZ}\} \end{aligned} \tag{2}$$

Equation (2) is another approach to estimate the CBS limit for the QCISD(T) method but the extrapolation starts from double zeta (DZ) to TZ basis sets and then considers the

difference in MP2 calculations. MP2 (second-order Møller–Plesset perturbation theory correction) is another method used for including electron correlation effects, where

$$\begin{aligned} E[QCISD(T)/CBS]_{DZ\rightarrow TZ} = E[QCISD(T)/TZ] + \{E[QCISD(T)/TZ] \\ -E[QCISD(T)/DZ]\} \times 0.4629 \end{aligned} \quad (3)$$

Equation (3) is similar to Equation (1) but it uses DZ and TZ basis sets for QCISD(T) extrapolation. The scaling factor 0.4629 is used for adjusting the extrapolation from DZ to TZ.

$$E[MP2/CBS]_{TZ\rightarrow QZ} = E[MP2/QZ] + \{E[MP2/QZ] - E[MP2/TZ]\} \times 0.6938 \quad (4)$$

Equation (4) estimates the CBS limit using MP2, extrapolating from TZ to QZ. The scaling factor 0.6938 is consistent with Equation (1), reflecting the systematic approach in these extrapolations.

$$E[MP2/CBS]_{DZ\rightarrow TZ} = E[MP2/TZ] + \{E[MP2/TZ] - E[MP2/DZ]\} \times 0.4629 \quad (5)$$

Equation (5) is the MP2 method equivalent of Equation (3), using DZ and TZ basis sets for extrapolation. The scaling factor 0.4629 is consistent with Equation (3), reflecting the systematic approach in these extrapolations.

In summary, each of these equations plays a crucial role in computational chemistry, allowing for high-accuracy predictions of molecular energies by approximating the CBS limit using manageable basis sets. The scaling factors are empirically derived constants that help in fine-tuning the extrapolation process to yield results close to what would be obtained with an infinitely large basis set.

2.2.2. ONIOM[QCISD(T)/CBS] Single-Point Energies

The ONIOM[QCISD(T)/CBS] method, as proposed by Zhang and Zhang [32], has been validated for its accuracy and efficiency in large saturated and unsaturated biodiesel molecules [32,34,63]. This method constructs a reaction system by defining two layers, each treated at different theoretical levels. The high-level layer, known as the chemically active portion (CAP), is treated at the QCISD(T)/CBS level. In contrast, the low-level layer is treated at the DFT/6-311++G(d,p) level. A crucial aspect of the ONIOM method is the appropriate definition of the CAP, as it directly influences calculation accuracy and computational efficiency. The CAP includes the CH_2 (or CH_3) group under attack, the attacking radicals, and the neighboring groups. The efficacy of this approach, including the choice of link atoms, has been substantiated [32,34]. For the present study, CAP (2,2) is minimally required, which encompasses the CH_2 (or CH_3) group under attack and up to two neighboring groups on both sides, if they exist. Figure 1 illustrates a representative schematic for the hydrogen abstraction reactions of *n*-$C_{16}H_{34}$ + (H, OH, and HO_2) using the ONIOM method with CAP(2,2).

The ONIOM method predicts the energy of the entire system by calculating the low-level energy and then applying corrections for the difference in the chemically active portion (CAP) between the high-level and low-level calculations.

$$E^{ONIOM}[High : Low] = E^{Low}(R) + E^{High}(CAP) - E^{Low}(CAP) \quad (6)$$

Using the DFT/6-311++G(d,p) method for the low-level calculations and the $[QCISD(T)/CBS]_2$ method for the high-level, the ONIOM energies are calculated as

$$\begin{aligned} E^{ONIOM}[QCISD(T)CBS : DFT] = E^{ONIOM}[QCISD(T)/CBS : DFT]_{DZ\rightarrow TZ} \\ +\left\{E^{ONIOM}\left[MP2/CBS : DFT\right]_{TZ\rightarrow QZ} - E^{ONIOM}[MP2/CBS : DFT]_{DZ\rightarrow TZ}\right\} \end{aligned} \quad (7)$$

where

$$\begin{aligned} &E^{ONIOM}\left[QCISD(T)/CBS:DFT\right]_{DZ\to TZ} = E^{ONIOM}[QCISD(T)/TZ:DFT] \\ &+\left\{E^{ONIOM}[QCISD(T)/TZ:DFT] - E^{ONIOM}[QCISD(T)/DZ:DFT]\right\} \times 0.4629 \end{aligned} \quad (8)$$

$$\begin{aligned} &E^{ONIOM}\left[MP2/CBS:DFT\right]_{TZ\to QZ} = E^{ONIOM}[MP2/QZ:DFT] \\ &+\left\{E^{ONIOM}[MP2/QZ:DFT] - E^{ONIOM}[MP2/TZ:DFT]\right\} \times 0.6938 \end{aligned} \quad (9)$$

$$\begin{aligned} &E^{ONIOM}\left[MP2/CBS:DFT\right]_{DZ\to TZ} = E^{ONIOM}[MP2/TZ:DFT] \\ &+\left\{E^{ONIOM}[MP2/TZ:DFT] - E^{ONIOM}[MP2/DZ:DFT]\right\} \times 0.4629 \end{aligned} \quad (10)$$

The energy barrier (denoted as EB hereinafter) and the heat of reaction (denoted as ΔH hereinafter), including ZPE corrections, are calculated by

$$\begin{aligned} EB = &\left(E^{ONIOM}[QCISD(T)/CBS:DFT] + ZPE\right)_{\text{transition state}} \\ &-\left(E^{ONIOM}[QCISD(T)/CBS:DFT] + ZPE\right)_{\text{reactants}} \end{aligned} \quad (11)$$

$$\begin{aligned} \Delta H = &\left(E^{ONIOM}[QCISD(T)/CBS:DFT] + ZPE\right)_{\text{products}} \\ &-\left(E^{ONIOM}[QCISD(T)/CBS:DFT] + ZPE\right)_{\text{reactants}} \end{aligned} \quad (12)$$

All the calculations in the present study were performed using the Gaussian 09 program package [64].

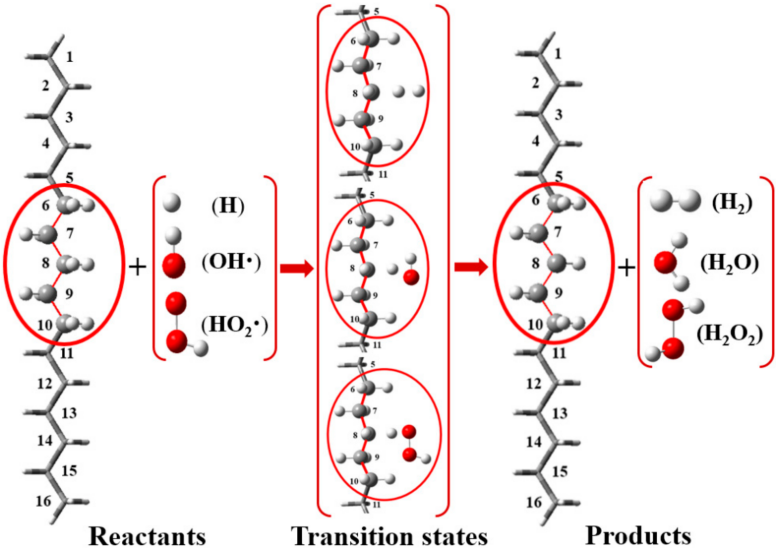

Figure 1. Illustration of the ONIOM[QCISD(T)/CBS:DFT]/CAP(2,2) method for the hydrogen abstraction reactions of straight-chain alkanes, *n*-$C_{16}H_{34}$ + (H, OH, and HO_2) → $CH_3(CH_2)_4CH(CH_2)_5CH_3$ + (H_2, H_2O, and H_2O_2). The indices from 1 to 16 denote the CH_3 (or CH_2) groups. CAP (2,2) (in red circle) represents the chemically active portion consisting of the No.6 and No.7 CH_2 groups on one side of the No. 8 CH_2 group under H, OH, and HO_2 radical attack, and No. 9 and No. 10 CH_2 groups on the other side of No. 8 CH_2 group in reactant and products. For the transition states, H, OH, and HO_2 radicals are also needed to be added to the CAP.

3. Results and Discussion

3.1. Hydrogen Abstraction Reactions of n-C_nH_{2n+2} + H (n = 1–16)

3.1.1. Validation and Comparison of Two [QCISD(T)/CBS] Methods

For the relatively small molecules, the two high-level methods are computationally affordable and have been used to establish benchmark data for validating the present ONIOM

method. For the n-C_nH_{2n+2} + H reactions, validation can be achieved up to n = 5 using [QCISD(T)/CBS]$_1$ and up to n = 9 with [QCISD(T)/CBS]$_2$. It is seen that [QCISD(T)/CBS]$_2$ generally predicts slightly lower energies (EB and ΔH) compared to [QCISD(T)/CBS]$_1$. The computational differences (absolute values) between these two [QCISD(T)/CBS] methods are generally less than 0.10 kcal/mol, as indicated in Table 1. The only exception is the reaction H-R1, where the differences between the two methods are −0.11 kcal/mol for EB and −0.15 kcal/mol for ΔH.

Table 1. The comparison of calculated results (EB and ΔH) and the differences ([QCISD(T)/CBS]$_2$ relative to [QCISD(T)/CBS]$_1$) for the hydrogen abstraction reactions of n-C_nH_{2n+2} + H (n = 1−5) using the [QCISD(T)/CBS]$_1$ and [QCISD(T)/CBS]$_2$ (unit: kcal/mol).

	No.	Reactions	EB			ΔH		
			[QCISD(T)/CBS]$_1$	[QCISD(T)/CBS]$_2$	Difference	[QCISD(T)/CBS]$_1$	[QCISD(T)/CBS]$_2$	Difference
C1	H-R1	$H + CH_4 \rightarrow H_2 + CH_3$	13.45	13.34	−0.11	−0.15	−0.30	−0.15
C2	H-R2	$H + CH_3CH_3 \rightarrow H_2 + CH_2CH_3$	10.27	10.17	−0.10	−3.96	−4.05	−0.09
C3	H-R3	$H + CH_3CH_2CH_3 \rightarrow H_2 + CH_2CH_2CH_3$	10.21	10.11	−0.10	−3.58	−3.66	−0.08
	H-R4	$H + CH_3CH_2CH_3 \rightarrow H_2 + CH_3CHCH_3$	7.58	7.49	−0.09	−6.72	−6.74	−0.02
C4	H-R5	$H + CH_3(CH_2)_2CH_3 \rightarrow H_2 + CH_2(CH_2)_2CH_3$	10.11	10.01	−0.10	−3.64	−3.73	−0.09
	H-R6	$H + CH_3(CH_2)_2CH_3 \rightarrow H_2 + CH_3CHCH_2CH_3$	7.47	7.39	−0.08	−6.43	−6.45	−0.02
	H-R7	$H + CH_3(CH_2)_3CH_3 \rightarrow H_2 + CH_2(CH_2)_3CH_3$	10.04	9.95	−0.09	−3.61	−3.69	−0.08
C5	H-R8	$H + CH_3(CH_2)_3CH_3 \rightarrow H_2 + CH_3CH(CH_2)_2CH_3$	7.46	7.38	−0.08	−6.43	−6.45	−0.02
	H-R9	$H + CH_3(CH_2)_3CH_3 \rightarrow H_2 + CH_3CH_2CHCH_2CH_3$	7.46	7.38	−0.08	−6.11	−6.13	−0.02

3.1.2. Validation of ONIOM Energies of n-C_nH_{2n+2} + H (n = 1–9)

Through the comparison between the two [QCISD(T)/CBS] methods, it is evident that the [QCISD(T)/CBS]$_2$ method can be considered a high-level method for validating the ONIOM method in systems with more than five nonhydrogen atoms. These systems are computationally expensive for the [QCISD(T)/CBS]$_1$ method. Therefore, we compared the calculated results (EB and ΔH) for n-C_nH_{2n+2} + H (n = 1–9) using both the ONIOM[QCISD(T)/CBS:DFT] and [QCISD(T)/CBS]$_2$ methods for a total of 25 reactions (referred to as H-R1 to H-R25, as shown in Table 2). It is observed that the ONIOM method consistently predicts slightly higher energies than the [QCISD(T)/CBS]$_2$ method. The computational differences between these two methods are generally less than 0.10 kcal/mol, as detailed in Figure 2 and Table 2, except for the reaction H-R25, which shows a difference of 0.12 kcal/mol. A slightly augmented CAP(3,3) should be able to reduce the relative error in the case of H-R25.

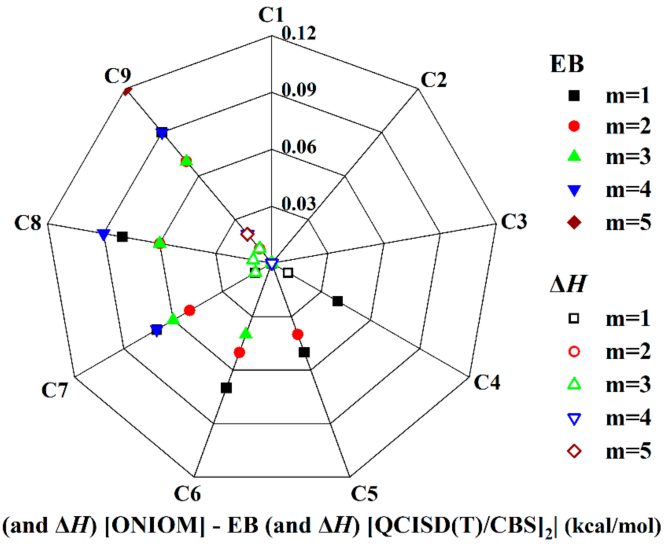

Figure 2. The difference in the calculated energy barriers (EB) and heat of reactions (ΔH) for the reactions of n-C_nH_{2n+2} + H (n = 1–9); the notation m (= 1–5) denotes the group under H atom attack.

Table 2. The comparison of calculated results (EB and Δ*H*) the differences (ONIOM relative to [QCISD(T)/CBS]$_2$) for the hydrogen abstraction reactions of *n*-C_nH_{2n+2} + H (*n* = 1−9) using the [QCISD(T)/CBS]$_2$ and ONIOM (unit: kcal/mol).

	No.	Reactions	EB			Δ*H*		
			[QCISD(T)/CBS]$_2$	ONIOM	Difference	[QCISD(T)/CBS]$_2$	ONIOM	Difference
C1	H-R1	$H + CH_4 \rightarrow H_2 + CH_3$	13.34	13.34	0.00	−0.30	−0.30	0.00
C2	H-R2	$H + CH_3CH_3 \rightarrow H_2 + CH_2CH_3$	10.17	10.17	0.00	−4.05	−4.05	0.00
C3	H-R3	$H + CH_3CH_2CH_3 \rightarrow H_2 + CH_2CH_2CH_3$	10.11	10.11	0.00	−3.66	−3.66	0.00
	H-R4	$H + CH_3CH_2CH_3 \rightarrow H_2 + CH_3CHCH_3$	7.49	7.49	0.00	−6.74	−6.74	0.00
C4	H-R5	$H + CH_3(CH_2)_2CH_3 \rightarrow H_2 + CH_2(CH_2)_2CH_3$	10.01	10.05	0.04	−3.73	−3.72	0.01
	H-R6	$H + CH_3(CH_2)_2CH_3 \rightarrow H_2 + CH_3CHCH_2CH_3$	7.39	7.39	0.00	−6.45	−6.45	0.00
C5	H-R7	$H + CH_3(CH_2)_3CH_3 \rightarrow H_2 + CH_2(CH_2)_3CH_3$	9.95	10.00	0.05	−3.69	−3.69	0.00
	H-R8	$H + CH_3(CH_2)_3CH_3 \rightarrow H_2 + CH_3CH(CH_2)_2CH_3$	7.38	7.42	0.04	−6.45	−6.45	0.00
	H-R9	$H + CH_3(CH_2)_3CH_3 \rightarrow H_2 + CH_3CH_2CHCH_2CH_3$	7.38	7.38	0.00	−6.13	−6.13	0.00
C6	H-R10	$H + CH_3(CH_2)_4CH_3 \rightarrow H_2 + CH_2(CH_2)_4CH_3$	9.91	9.98	0.07	−3.72	−3.72	0.00
	H-R11	$H + CH_3(CH_2)_4CH_3 \rightarrow H_2 + CH_3CH(CH_2)_3CH_3$	7.39	7.44	0.05	−6.49	−6.49	0.00
	H-R12	$H + CH_3(CH_2)_4CH_3 \rightarrow H_2 + CH_3CH_2CH(CH_2)_2CH_3$	7.28	7.32	0.04	−6.19	−6.19	0.00
C7	H-R13	$H + CH_3(CH_2)_5CH_3 \rightarrow H_2 + CH_2(CH_2)_5CH_3$	9.92	9.99	0.07	−3.71	−3.70	0.01
	H-R14	$H + CH_3(CH_2)_5CH_3 \rightarrow H_2 + CH_3CH(CH_2)_4CH_3$	7.33	7.38	0.05	−6.47	−6.47	0.00
	H-R15	$H + CH_3(CH_2)_5CH_3 \rightarrow H_2 + CH_3CH_2CH(CH_2)_3CH_3$	7.22	7.28	0.06	−6.17	−6.18	−0.01
	H-R16	$H + CH_3(CH_2)_5CH_3 \rightarrow H_2 + CH_3(CH_2)_2CH(CH_2)_2CH_3$	7.23	7.30	0.07	−6.21	−6.21	0.00
C8	H-R17	$H + CH_3(CH_2)_6CH_3 \rightarrow H_2 + CH_2(CH_2)_6CH_3$	9.86	9.94	0.08	−3.71	−3.71	0.00
	H-R18	$H + CH_3(CH_2)_6CH_3 \rightarrow H_2 + CH_3CH(CH_2)_5CH_3$	7.28	7.34	0.06	−6.48	−6.48	0.00
	H-R19	$H + CH_3(CH_2)_6CH_3 \rightarrow H_2 + CH_3CH_2CH(CH_2)_4CH_3$	7.15	7.21	0.06	−6.17	−6.18	−0.01
	H-R20	$H + CH_3(CH_2)_6CH_3 \rightarrow H_2 + CH_3(CH_2)_2CH(CH_2)_3CH_3$	7.13	7.22	0.09	−6.24	−6.24	0.00
C9	H-R21	$H + CH_3(CH_2)_7CH_3 \rightarrow H_2 + CH_2(CH_2)_7CH_3$	9.77	9.86	0.09	−3.70	−3.70	0.00
	H-R22	$H + CH_3(CH_2)_7CH_3 \rightarrow H_2 + CH_3CH(CH_2)_6CH_3$	7.13	7.20	0.07	−6.46	−6.47	−0.01
	H-R23	$H + CH_3(CH_2)_7CH_3 \rightarrow H_2 + CH_3CH_2CH(CH_2)_5CH_3$	7.02	7.09	0.07	−6.17	−6.18	−0.01
	H-R24	$H + CH_3(CH_2)_7CH_3 \rightarrow H_2 + CH_3(CH_2)_2CH(CH_2)_4CH_3$	7.01	7.10	0.09	−6.23	−6.25	−0.02
	H-R25	$H + CH_3(CH_2)_7CH_3 \rightarrow H_2 + CH_3(CH_2)_3CH(CH_2)_3CH_3$	6.92	7.04	0.12	−6.20	−6.22	−0.02

3.1.3. ONIOM Energies of *n*-C_nH_{2n+2} + H (*n* = 10–16)

After validating the accuracy of the ONIOM method, we applied it to study larger reaction systems involving *n*-C_nH_{2n+2} + H (*n* = 10–16) at various (all) hydrogen abstraction sites. This study encompassed a total of 47 reactions (referred to as H-R26 to H-R72, as shown in Table S1 of the Supplementary Materials). These reactions have not been previously studied using high-level methods. The calculated energies, EB and Δ*H*, are presented in Figure 3 and Table S1 of the Supplementary Materials. Several observations can be drawn from these results:

The hydrogen abstraction reactions occurring at CH_3 groups, denoted by 1 at the reaction site, exhibit the highest EBs, approximately 9.80 kcal/mol, ranging from 9.78 to 9.82 kcal/mol. These reactions also have the highest (negative) Δ*H*s, around −3.71 kcal/mol, with a range from −3.72 to −3.70 kcal/mol.

The hydrogen abstraction reactions occurring at CH_2 groups, denoted by 2 to 8 at the reaction sites, display nearly identical EBs, approximately 7.05 kcal/mol, with a range from 6.93 to 7.21 kcal/mol. The Δ*H*s of these reactions are around −6.30 kcal/mol, varying from −6.49 to −6.16 kcal/mol.

The variation in energies (EBs and Δ*H*s) for *n*-C_nH_{2n+2} + H (*n* = 10–16) in the hydrogen abstraction reactions at CH_3 and CH_2 groups is negligible. This is indicated by the coefficients of variation ($C_v = \left|\frac{\sigma}{\mu}\right|$, σ is standard deviation and μ is arithmetic mean). For the CH_3 groups, the C_v values are 0.2% for EB and 0.2% for Δ*H*. For the CH_2 groups, these values are 1.0% for EB and 1.5% for Δ*H*.

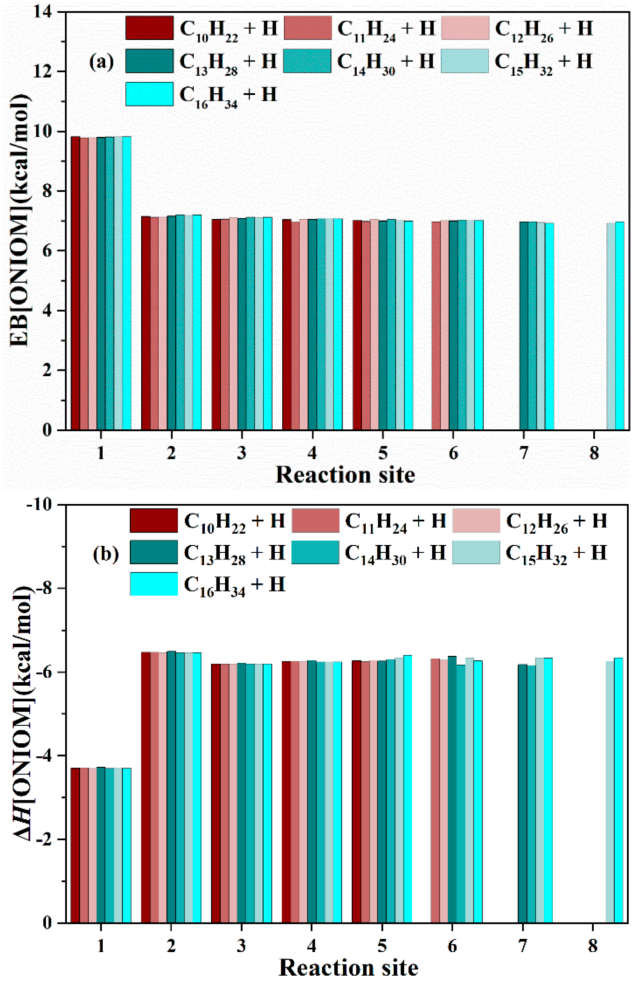

Figure 3. (**a**) The predicted EBs and (**b**) the predicted Δ*H*s for the hydrogen abstraction reactions of *n*-C_nH_{2n+2} + H (*n* = 10–16).

3.2. Hydrogen Abstraction Reactions of n-C_nH_{2n+2} + OH (n = 1–16)

We opted for the M06-2X/6-311++G(d,p) method to study the reaction systems of *n*-C_nH_{2n+2} + OH because we found the imaginary frequencies of *n*-C_nH_{2n+2} + OH at the B3LYP/6-311++G(d,p) level are relatively smaller than those of *n*-C_nH_{2n+2} + H and *n*-C_nH_{2n+2} + HO_2 at the same theoretical level. For instance, using C_3H_8 as an example, the imaginary frequencies of the transition states for the reactions occurring at methyl group are 207.77i cm^{-1} for OH-R3, 1160.15i cm^{-1} for H-R3, and 1649.88i cm^{-1} for HO_2-R3. When the reactions occur at other reaction sites, the imaginary frequencies of the transition states for *n*-C_nH_{2n+2} + OH decrease significantly, for example, 44.96i cm^{-1} for OH-R4 compared to 1123.81i cm^{-1} for H-R4 and 1663.22i cm^{-1} for HO_2-R4. Due to these relatively small imaginary frequencies for *n*-C_nH_{2n+2} + OH, confirming the transition state using IRC becomes challenging. Therefore, we employed the M06-2X method with the 6-311++G(d,p) basis set for all reactions of *n*-C_nH_{2n+2} + OH (*n* = 1–16). Revisiting the C_3H_8 as an example, the imaginary frequencies for the transition states of OH-R3 and OH-R4 using this method are 788.88i cm^{-1} and 535.31i cm^{-1}, respectively.

3.2.1. Validation and Comparison of Two [QCISD(T)/CBS] Methods

For the reactions of *n*-C_nH_{2n+2} + OH, validation can be achieved up to *n* = 4 using the $[QCISD(T)/CBS]_1$ method and up to *n* = 8 with the $[QCISD(T)/CBS]_2$ method. In contrast to the system of *n*-C_nH_{2n+2} + H (*n* = 1–5), the $[QCISD(T)/CBS]_2$ method consistently predicts higher EBs and lower Δ*H*s compared to the $[QCISD(T)/CBS]_1$ method for *n*-C_nH_{2n+2} + OH (*n* = 1–4). The computational differences (absolute values) between

these two [QCISD(T)/CBS] methods are generally less than 0.20 kcal/mol for EB and 0.10 kcal/mol for Δ*H*, as indicated in Table 3.

Table 3. The comparison of calculated results (EB and Δ*H*) and the differences ($[QCISD(T)/CBS]_2$ relative to $[QCISD(T)/CBS]_1$) for the hydrogen abstraction reactions of *n*-C_nH_{2n+2} + OH (*n* = 1−4) using the $[QCISD(T)/CBS]_1$ and $[QCISD(T)/CBS]_2$ (unit: kcal/mol).

	No.	Reactions	EB			Δ*H*		
			$[QCISD(T)/CBS]_1$	$[QCISD(T)/CBS]_2$	Difference	$[QCISD(T)/CBS]_1$	$[QCISD(T)/CBS]_2$	Difference
C1	OH-R1	$OH + CH_4 \rightarrow H_2O + CH_3$	4.83	5.02	0.19	−14.84	−14.97	−0.13
C2	OH-R2	$OH + CH_3CH_3 \rightarrow H_2O + CH_2CH_3$	2.43	2.63	0.20	−18.42	−18.48	−0.06
C3	OH-R3	$OH + CH_3CH_2CH_3 \rightarrow H_2O + CH_2CH_2CH_3$	1.63	1.81	0.18	−18.40	−18.46	−0.06
	OH-R4	$OH + CH_3CH_2CH_3 \rightarrow H_2O + CH_3CHCH_3$	0.29	0.49	0.20	−21.47	−21.47	0.00
C4	OH-R5	$OH + CH_3(CH_2)_2CH_3 \rightarrow H_2O + CH_2(CH_2)_2CH_3$	2.72	2.88	0.16	−17.29	−17.36	−0.07
	OH-R6	$OH + CH_3(CH_2)_2CH_3 \rightarrow H_2O + CH_3CHCH_2CH_3$	0.81	0.99	0.18	−20.27	−20.27	0.00

3.2.2. Validation of ONIOM Energies of *n*-C_nH_{2n+2} + OH (*n* = 1–8)

We adopted the $[QCISD(T)/CBS]_2$ method to validate the ONIOM method for *n*-C_nH_{2n+2} + OH (*n* = 1–8). A total of 20 reactions (referred to as OH-R1 to OH-R20, as shown in Table 4) were compared. Similar to the systems of *n*-C_nH_{2n+2} + H (*n* = 1–9), the ONIOM method consistently predicts slightly higher EBs than the $[QCISD(T)/CBS]_2$ method. However, it predicts almost negligibly smaller Δ*H*s compared to the latter. The computational differences (absolute values) between these two methods are less than 0.10 kcal/mol for EB and 0.04 kcal/mol for Δ*H*, as indicated in Figure 4 and Table 4.

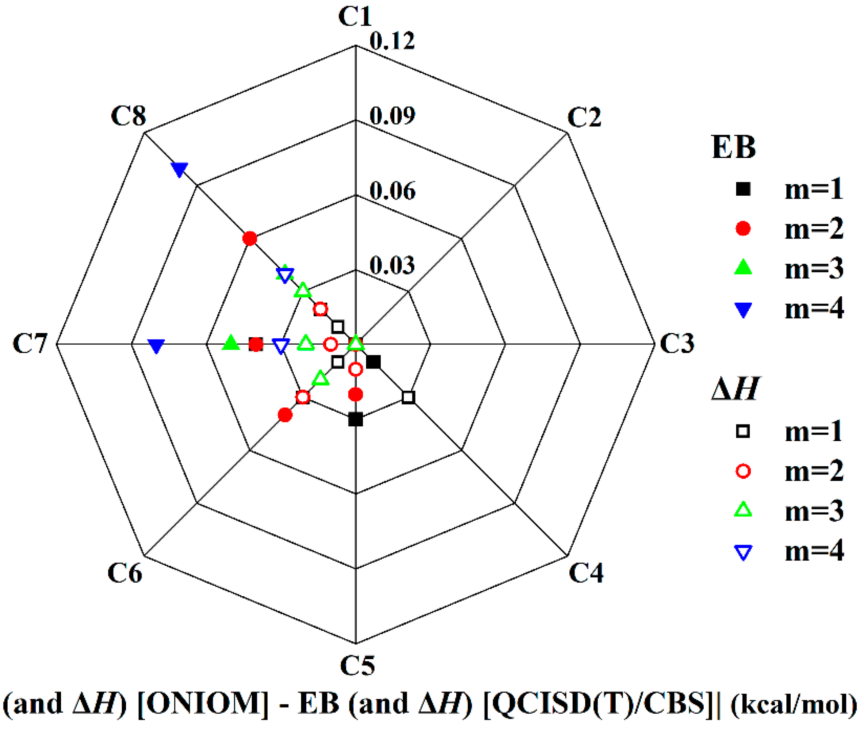

Figure 4. The difference in the calculated energy barriers (EB) and heat of reactions (Δ*H*) for the reactions of *n*-C_nH_{2n+2} + OH (*n* = 1–8); the notation m (= 1–4) denotes the group under OH radical attack.

Table 4. The comparison of calculated results (EB and Δ*H*) and the differences (ONIOM relative to [QCISD(T)/CBS]$_2$) for the hydrogen abstraction reactions of *n*-C_nH_{2n+2} + OH (*n* = 1–8) using the [QCISD(T)/CBS]$_2$ and ONIOM (unit: kcal/mol).

	No.	Reactions	EB			Δ*H*		
			[QCISD(T)/CBS]$_2$	ONIOM	Difference	[QCISD(T)/CBS]$_2$	ONIOM	Difference
C1	OH-R1	$OH + CH_4 \rightarrow H_2O + CH_3$	5.02	5.02	0.00	−14.97	−14.97	0.00
C2	OH-R2	$OH + CH_3CH_3 \rightarrow H_2O + CH_2CH_3$	2.63	2.63	0.00	−18.48	−18.48	0.00
C3	OH-R3	$OH + CH_3CH_2CH_3 \rightarrow H_2O + CH_2CH_2CH_3$	1.81	1.81	0.00	−18.46	−18.46	0.00
	OH-R4	$OH + CH_3CH_2CH_3 \rightarrow H_2O + CH_3CHCH_3$	0.49	0.49	0.00	−21.47	−21.47	0.00
C4	OH-R5	$OH + CH_3(CH_2)_2CH_3 \rightarrow H_2O + CH_2(CH_2)_2CH_3$	2.88	2.89	0.01	−17.36	−17.39	−0.03
	OH-R6	$OH + CH_3(CH_2)_2CH_3 \rightarrow H_2O + CH_3CHCH_2CH_3$	0.99	0.99	0.00	−20.27	−20.27	0.00
C5	OH-R7	$OH + CH_3(CH_2)_3CH_3 \rightarrow H_2O + CH_2(CH_2)_3CH_3$	1.95	1.98	0.03	−18.59	−18.59	0.00
	OH-R8	$OH + CH_3(CH_2)_3CH_3 \rightarrow H_2O + CH_3CH(CH_2)_2CH_3$	−0.29	−0.27	0.02	−21.29	−21.30	−0.01
	OH-R9	$OH + CH_3(CH_2)_3CH_3 \rightarrow H_2O + CH_3CH_2CHCH_2CH_3$	−0.13	−0.13	0.00	−20.93	−20.93	0.00
C6	OH-R10	$OH + CH_3(CH_2)_4CH_3 \rightarrow H_2O + CH_2(CH_2)_4CH_3$	1.92	1.95	0.03	−18.12	−18.13	−0.01
	OH-R11	$OH + CH_3(CH_2)_4CH_3 \rightarrow H_2O + CH_3CH(CH_2)_3CH_3$	0.37	0.41	0.04	−20.81	−20.84	−0.03
	OH-R12	$OH + CH_3(CH_2)_4CH_3 \rightarrow H_2O + CH_3CH_2CH(CH_2)_2CH_3$	0.26	0.28	0.02	−20.52	−20.54	−0.02
C7	OH-R13	$OH + CH_3(CH_2)_5CH_3 \rightarrow H_2O + CH_2(CH_2)_5CH_3$	1.64	1.68	0.03	−18.55	−18.55	0.00
	OH-R14	$OH + CH_3(CH_2)_5CH_3 \rightarrow H_2O + CH_3CH(CH_2)_4CH_3$	−0.17	−0.13	0.04	−21.67	−21.68	−0.01
	OH-R15	$OH + CH_3(CH_2)_5CH_3 \rightarrow H_2O + CH_3CH_2CH(CH_2)_3CH_3$	−0.79	−0.74	0.05	−20.94	−20.96	−0.02
	OH-R16	$OH + CH_3(CH_2)_5CH_3 \rightarrow H_2O + CH_3(CH_2)_2CH(CH_2)_2CH_3$	−0.94	−0.86	0.08	−21.40	−21.43	−0.03
C8	OH-R17	$OH + CH_3(CH_2)_6CH_3 \rightarrow H_2O + CH_2(CH_2)_6CH_3$	2.29	2.31	0.02	−18.39	−18.40	−0.01
	OH-R18	$OH + CH_3(CH_2)_6CH_3 \rightarrow H_2O + CH_3CH(CH_2)_5CH_3$	−0.14	−0.08	0.06	−21.14	−21.16	−0.02
	OH-R19	$OH + CH_3(CH_2)_6CH_3 \rightarrow H_2O + CH_3CH_2CH(CH_2)_4CH_3$	−0.24	−0.20	0.04	−20.94	−20.97	−0.03
	OH-R20	$OH + CH_3(CH_2)_6CH_3 \rightarrow H_2O + CH_3(CH_2)_2CH(CH_2)_3CH_3$	−0.86	−0.76	0.10	−20.89	−20.93	−0.04

3.2.3. ONIOM Energies of *n*-C_nH_{2n+2} + OH (*n* = 9–16)

We utilized the ONIOM method to investigate the larger reaction systems of *n*-C_nH_{2n+2} + OH (*n* = 9–16), examining all hydrogen abstraction sites. This study encompassed a total of 52 reactions (referred to as OH-R21 to OH-R72, as shown in Table S2 of the Supplementary Materials). These reactions have not been previously explored using high-level methods. The calculated energies, EB and Δ*H*, are presented in Figure 5 and Table S2 of the Supplementary Materials. Several observations can be drawn from these results, as follows:

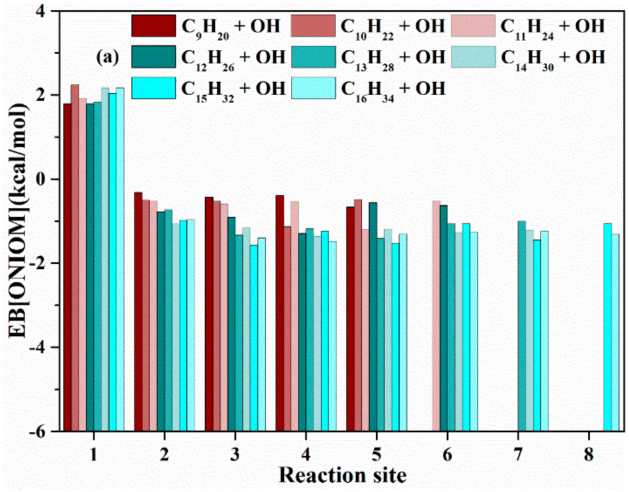

Figure 5. *Cont.*

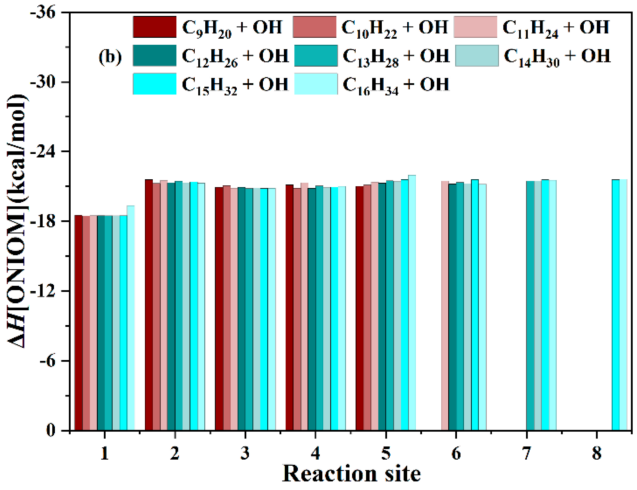

Figure 5. (**a**) The predicted EBs and (**b**) the predicted Δ*H*s for the hydrogen abstraction reactions of *n*-C_nH_{2n+2} + OH (*n* = 9–16).

The hydrogen abstraction reactions occurring at the CH_3 groups, denoted by 1 at the reaction site, exhibit the highest EBs, approximately 2.00 kcal/mol, with a range from 1.79 to 2.24 kcal/mol. These reactions also have the highest (negative) Δ*H*s, around −18.59 kcal/mol, ranging from −19.35 to −18.46 kcal/mol.

The hydrogen abstraction reactions occurring at CH_2 groups, denoted by 2 to 8 at the reaction sites, show fluctuating EBs, ranging from −1.57 to −0.32 kcal/mol, averaging around −1.00 kcal/mol. The Δ*H*s for these reactions are relatively consistent, approximately −21.25 kcal/mol, with a range from −21.98 to −20.82 kcal/mol.

For *n*-C_nH_{2n+2} + OH (*n* = 9–16), significant variations are observed in the EBs for the hydrogen abstraction reactions at CH_3 groups, with a coefficient of variation (C_v) of 8.5%, and at CH_2 groups with a C_v of 36.1%. This finding indicates that approximating the EBs for hydrogen abstraction from the CH_2 group by OH as a constant could lead to substantial errors in chemical kinetics calculations. In contrast, the variation in Δ*H*s is negligible, as indicated by C_v of 1.5% for the CH_3 groups and 1.3% for the CH_2 groups.

3.3. Hydrogen Abstraction Reactions of n-C_nH_{2n+2} + HO_2 (n = 1–16)

3.3.1. Validation and Comparison of Two [QCISD(T)/CBS] Methods

For *n*-C_nH_{2n+2} + HO_2, the reactions can be validated up to *n* = 3 using the $[QCISD(T)/CBS]_1$ method and up to 7 with the $[QCISD(T)/CBS]_2$ method. Similar to the systems of *n*-C_nH_{2n+2} + H (*n* = 1–5), the $[QCISD(T)/CBS]_2$ method consistently predicts lower energies (both EBs and Δ*H*s) than ($[QCISD(T)/CBS]_1$ for *n*-C_nH_{2n+2} + HO_2 (*n* = 1–3). The computational differences (absolute values) between these two [QCISD(T)/CBS] methods are generally less than 0.11 kcal/mol, as indicated in Table 5. The only exception is the reaction HO_2-R1, where the differences between the two methods are −0.18 kcal/mol for EB and −0.17 kcal/mol for Δ*H*.

Table 5. The comparison of calculated results (EB and Δ*H*) and the differences ($[QCISD(T)/CBS]_2$ relative to $[QCISD(T)/CBS]_1$) for the hydrogen abstraction reactions of *n*-C_nH_{2n+2} + HO_2 (*n* = 1–3) using the $[QCISD(T)/CBS]_1$ and $[QCISD(T)/CBS]_2$ (unit: kcal/mol).

	No.	Reactions	EB			Δ*H*		
			$[QCISD(T)/CBS]_1$	$[QCISD(T)/CBS]_2$	Difference	$[QCISD(T)/CBS]_1$	$[QCISD(T)/CBS]_2$	Difference
C1	HO_2-R1	$HO_2 + CH_4 \rightarrow H_2O_2 + CH_3$	24.29	24.11	−0.18	17.21	17.04	−0.17
C2	HO_2-R2	$HO_2 + CH_3CH_3 \rightarrow H_2O_2 + CH_2CH_3$	20.01	19.90	−0.11	13.40	13.29	−0.11
C3	HO_2-R3	$HO_2 + CH_3CH_2CH_3 \rightarrow H_2O_2 + CH_2CH_2CH_3$	19.51	19.40	−0.09	13.78	13.68	−0.10
	HO_2-R4	$HO_2 + CH_3CH_2CH_3 \rightarrow H_2O_2 + CH_3CHCH_3$	16.92	16.86	−0.06	10.64	10.60	−0.04

3.3.2. Validation of ONIOM Energies of C_nH_{2n+2} + HO_2 (n = 1–7)

We adopted the [QCISD(T)/CBS]$_2$ method to validate the ONIOM method for n-C_nH_{2n+2} + HO_2 (n = 1–7), encompassing a total of 16 reactions (referred to as HO_2-R1 to HO_2-R16 in Table 6). Consistent with expectations, the ONIOM method predicts slightly larger energies (both EBs and ΔHs) compared to the [QCISD(T)/CBS]$_2$ method. The computational differences between these two methods are generally less than 0.07 kcal/mol for EB and 0.01 kcal/mol for ΔH, as illustrated in Figure 6 and Table 6. The slightly large discrepancy of 0.11 kcal/mol for HO_2-R16 is likely due to CAP(2,2) including almost all CH_2 groups except the two terminal methyl groups.

Table 6. The comparison of calculated results (EB and ΔH) and the differences (ONIOM relative to [QCISD(T)/CBS]$_2$) for the hydrogen abstraction reactions of n-C_nH_{2n+2} + HO_2 (n = 1–7) using the [QCISD(T)/CBS]$_2$ and ONIOM (unit: kcal/mol).

	No.	Reactions	EB			ΔH		
			[QCISD(T)/CBS]$_2$	ONIOM	Difference	[QCISD(T)/CBS]$_2$	ONIOM	Difference
C1	HO_2-R1	$HO_2 + CH_4 \rightarrow H_2O_2 + CH_3$	24.11	24.11	0.00	17.04	17.04	0.00
C2	HO_2-R2	$HO_2 + CH_3CH_3 \rightarrow H_2O_2 + CH_2CH_3$	19.90	19.90	0.00	13.29	13.29	0.00
C3	HO_2-R3	$HO_2 + CH_3CH_2CH_3 \rightarrow H_2O_2 + CH_2CH_2CH_3$	19.40	19.40	0.00	13.68	13.68	0.00
	HO_2-R4	$HO_2 + CH_3CH_2CH_3 \rightarrow H_2O_2 + CH_3CHCH_3$	16.86	16.86	0.00	10.60	10.60	0.00
C4	HO_2-R5	$HO_2 + CH_3(CH_2)_2CH_3 \rightarrow H_2O_2 + CH_2(CH_2)_2CH_3$	19.25	19.31	0.06	13.61	13.62	0.01
	HO_2-R6	$HO_2 + CH_3(CH_2)_2CH_3 \rightarrow H_2O_2 + CH_3CHCH_2CH_3$	16.37	16.37	0.00	10.89	10.89	0.00
C5	HO_2-R7	$HO_2 + CH_3(CH_2)_3CH_3 \rightarrow H_2O_2 + CH_2(CH_2)_3CH_3$	19.58	19.64	0.06	13.65	13.65	0.00
	HO_2-R8	$HO_2 + CH_3(CH_2)_3CH_3 \rightarrow H_2O_2 + CH_3CH(CH_2)_2CH_3$	16.24	16.29	0.05	10.89	10.89	0.00
	HO_2-R9	$HO_2 + CH_3(CH_2)_3CH_3 \rightarrow H_2O_2 + CH_3CH_2CHCH_2CH_3$	16.10	16.10	0.00	11.21	11.21	0.00
C6	HO_2-R10	$HO_2 + CH_3(CH_2)_4CH_3 \rightarrow H_2O_2 + CH_2(CH_2)_4CH_3$	19.52	19.58	0.06	13.62	13.62	0.00
	HO_2-R11	$HO_2 + CH_3(CH_2)_4CH_3 \rightarrow H_2O_2 + CH_3CH(CH_2)_3CH_3$	16.38	16.44	0.06	10.85	10.85	0.00
	HO_2-R12	$HO_2 + CH_3(CH_2)_4CH_3 \rightarrow H_2O_2 + CH_3CH_2CH(CH_2)_2CH_3$	15.99	16.05	0.06	11.15	11.15	0.00
C7	HO_2-R13	$HO_2 + CH_3(CH_2)_5CH_3 \rightarrow H_2O_2 + CH_2(CH_2)_5CH_3$	19.45	19.51	0.06	13.63	13.64	0.01
	HO_2-R14	$HO_2 + CH_3(CH_2)_5CH_3 \rightarrow H_2O_2 + CH_3CH(CH_2)_4CH_3$	16.16	16.22	0.06	10.87	10.87	0.00
	HO_2-R15	$HO_2 + CH_3(CH_2)_5CH_3 \rightarrow H_2O_2 + CH_3CH_2CH(CH_2)_3CH_3$	16.39	16.46	0.07	11.17	11.16	−0.01
	HO_2-R16	$HO_2 + CH_3(CH_2)_5CH_3 \rightarrow H_2O_2 + CH_3(CH_2)_2CH(CH_2)_2CH_3$	15.77	15.88	0.11	11.13	11.13	0.00

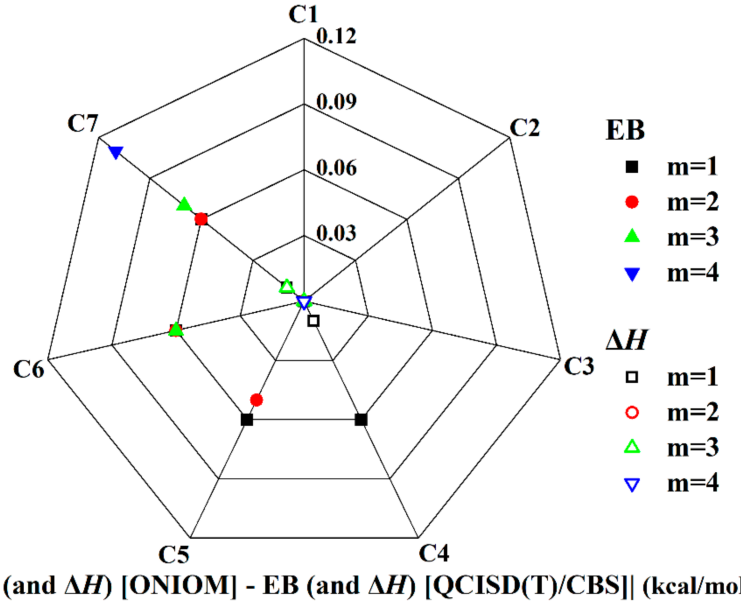

Figure 6. The difference in the calculated energy barriers (EB) and heat of reactions (ΔH) for the reactions of n-C_nH_{2n+2} + HO_2 (n = 1–7); the notation m (= 1–4) denotes the group under HO_2 radical attack.

3.3.3. ONIOM Energies of C_nH_{2n+2} + HO_2 (n = 8–16)

We applied the ONIOM method to study the larger reaction systems of n-C_nH_{2n+2} + HO_2 (n = 8–16) across all hydrogen abstraction sites. This study encompassed a total of 56 reactions (referred to as R17 to R72, as shown in Table S3 of the Supplementary Materials). These reactions have not been previously studied using high-level methods. The calculated energies, EB and ΔH, are presented in Figure 7 and Table S3 of the Supplementary Materials. Several observations can be drawn from these results, as follows:

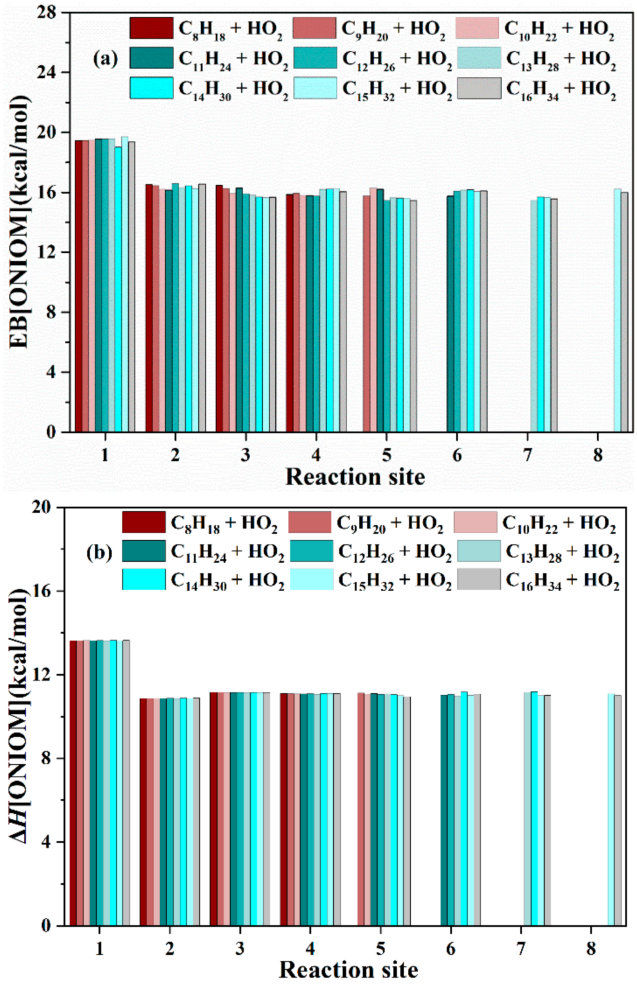

Figure 7. (**a**) The predicted EBs and (**b**) the predicted ΔHs for the hydrogen abstraction reactions of n-C_nH_{2n+2} + HO_2 (n = 8–16).

The hydrogen abstraction reactions occurring at the CH_3 groups, denoted by 1 at the reaction site, exhibit the highest EBs, approximately 19.45 kcal/mol, ranging from 19.00 to 19.69 kcal/mol. Additionally, these reactions have the highest ΔHs, around 13.63 kcal/mol, with a range from 13.62 to 13.64 kcal/mol.

The hydrogen abstraction reactions occurring at the CH_2 groups, denoted by 2 to 8 at the reaction site, show slight fluctuations in EBs, averaging around 15.99 kcal/mol, with a range from 15.45 to 16.58 kcal/mol. Additionally, these reactions exhibit almost the same ΔHs, approximately 11.05 kcal/mol, with a range from 10.85 to 11.18 kcal/mol.

For n-C_nH_{2n+2} + HO_2 (n = 8–16), the variation in energies (EBs and ΔHs) for the hydrogen abstraction reactions occurring at the CH_3 and CH_2 groups is negligible. This is indicated by the coefficients of variation (C_v), which are 0.9% for EB and 0.04% for ΔH in CH_3 groups, and 2.0% for EB and 0.9% for ΔH in the CH_2 groups.

3.4. Comparision with Literature Data

3.4.1. Comparison with Data from Kinetic Modelling

Practical kinetic modelling for large straight-chain alkane molecules primarily depends on empirical and semiempirical methods to establish thermochemical data in reaction mechanisms [65–68]. In these models, hydrogen abstraction reactions of straight-chain alkanes by H, OH, and HO_2 are mainly categorized into two types: reactions occurring at primary sites (CH_3 groups) and those at other sites (CH_2 groups), with the EBs being treated as constants for these two types. Due to its distinct behaviors of CH_4, which lacks the C-C bond existing in larger hydrocarbons, it is considered separately. When compared to calculated data obtained using the ONIOM method, the EBs in these kinetic models are generally underestimated for reactions of n-C_nH_{2n+2} + H and n-C_nH_{2n+2} + HO_2. However, for the reactions of n-C_nH_{2n+2} + OH, the EBs fall within the range of the data obtained by the ONIOM method, as indicated in Table 7.

Table 7. The comparison of EBs between kinetic modeling and the ONIOM method for the hydrogen abstraction reactions of n-C_nH_{2n+2} + H, OH, and HO_2 (n = 3–16) (unit: kcal/mol).

Involved Radical	Reaction Sites	ONIOM	Reference
H	Primary sites (CH3 groups)	9.78 to 10.11	7.70 [a], 7.70 [b], 8.61 [c]
	Other sites (CH_2 group)	6.93 to 7.49	5.00 [a], 5.00 [b], 5.93 [c]
OH	Primary sites (CH3 groups)	1.68 to 2.89	0.45 [a], 1.81 [b], 2.41 [c]
	Other sites (CH_2 group)	−1.57 to 0.99	−0.76 [a], 0.70 [b], 1.19 [c]
HO_2	Primary sites (CH3 groups)	19.00 to 19.69	17.00 [a], 19.41 [b]
	Other sites (CH_2 group)	15.45 to 16.86	15.49 [a], 17.02 [b]

[a] EB from Battin-Leclerc et al. [65]. [b] EB from Nehse et al. [66] [c] Calculated from Equation (13).

Cohen [38,39,69] employed the Evans–Polanyi principle [70] to calculate the activation energies by

$$E_{act} = \alpha(BDE_{C-H} - \beta) \quad (13)$$

where BDE is bond dissociation energy. The BDE values are derived from experimental data using the principle of group additivity. These values vary depending on the specific reaction site involved in the hydrogen abstraction reaction. It has been observed that BDE values differ for various molecules. For instance, BDE(CH_4) is 105.1 kcal/mol, while BDE(C_2H_6) is 100.6 kcal/mol. For the molecule larger than C_2H_6, the BDE for CH_3 groups is 100.5 kcal/mol, and for CH_2 groups, it is 97.1 kcal/mol [39].

In the study of H + alkane reactions [39], the values of α and β are set at 0.79 and 89.6 kcal/mol, respectively. Using these values in Equation (13), the calculated energies for n-C_nH_{2n+2} + H have been compared with the ONIOM energies, as shown in Table 7. It is observed that the EBs calculated by Equation (13) remain constants for reactions occurring at primary sites (CH_3 groups), with an EB of 8.61 kcal/mol, and at other reaction sites (CH_2 groups), with an EB of 5.93 kcal/mol, for molecules larger than C_2H_6. For CH_4 and C_2H_6, the EBs are 12.25 kcal/mol and 8.69 kcal/mol, respectively. Generally, these EBs calculated by Equation (13) are lower than those obtained using the ONIOM method.

In the study of OH + alkane reactions [38], the values of α and β are determined to be 0.36 and 93.8 kcal/mol, respectively. The energies of n-C_nH_{2n+2} + OH, calculated using Equation (13), have been compared with those obtained using the ONIOM method, as presented in Table 7. It is noted that the EBs calculated by Equation (13) remain constants for reactions occurring at primary sites (CH_3 groups), with an EB of 2.41 kcal/mol, and at other reaction sites (CH_2 groups), with an EB of 1.19 kcal/mol, for molecules larger than C_2H_6. For CH_4 and C_2H_6, the calculated EBs are 4.07 kcal/mol and 2.45 kcal/mol, respectively. Generally, these EBs calculated by Equation (13) are lower than the EBs for n-C_nH_{2n+2} + OH (n = 1–2) and higher than those for n-C_nH_{2n+2} + OH (n > 2) calculated using the ONIOM method.

3.4.2. Comparison with Data from Ab Initio Calculations

There are a few studies for the reactions of *n*-C_nH_{2n+2} molecules by H, OH, and HO_2 radicals using high-level methods, mainly focused on the smaller molecules.

For the reactions of *n*-C_nH_{2n+2} + H, Espinosa-Garcia [52] calculated the reaction of CH_4 with H atom at the CCSD(T)/cc-pVTZ//MP2(full)/6-31G(d,p) level, employing a scaling all the correlation energy (SAC) method [71]. Sivaramakrishnan et al. [49] analyzed the reaction systems of C_2H_6 and C_3H_8 at the CCSD(T)/aug-cc-pV∞Z//MP2/6-311++G(d,p) level. Peukert et al. [47] calculated the reaction system of *n*-C_4H_{10} and H atom at the CCSD(T)/cc-pV∞Z//M06-2X/cc-pVTZ level. The results, calculated using the ONIOM method for these systems, show good agreement with these high-level theoretical calculations, generally exhibiting differences of less than 0.2 kcal/mol, as illustrated in Table 8. For larger *n*-C_nH_{2n+2} + H reaction systems, Wang et al. [72] very recently studied the reaction of *n*-decane with H atom at the CBS-QB3//M06-2X/6-311++G(d,p) level, finding that the difference compared with the ONIOM method is generally less than 0.2 kcal/mol. Chi and You [73] investigated the reaction of *n*-$C_{18}H_{38}$ + H, using M06-2X/6-311++G(d,p). They concluded that the reaction occurring at CH_3 groups (H-R82) has the highest energy barrier (EB) of 10.85 kcal/mol, while the EBs for reactions at other positions range from 7.7 to 7.8 kcal/mol. A comparison of these results with those obtained using the ONIOM method is presented in Table 8. Their results for EBs are higher than the ONIOM results by 0.6 to 0.8 kcal/mol, except for the reaction H-R82, where the difference is 1.01 kcal/mol higher, as also indicated in Table 8.

Table 8. The calculated EBs for the hydrogen abstraction reactions of *n*-C_nH_{2n+2} + H (*n* = 1−4, 10, and 18) (unit: kcal/mol).

	No.	Reactions	ONIOM	Reference
C1	H-R1	$H + CH_4 \rightarrow H_2 + CH_3$	13.34	13.3 [a]
C2	H-R2	$H + CH_3CH_3 \rightarrow H_2 + CH_2CH_3$	10.17	10.30 [b]
C3	H-R3	$H + CH_3CH_2CH_3 \rightarrow H_2 + CH_2CH_2CH_3$	10.11	10.27 [b]
	H-R4	$H + CH_3CH_2CH_3 \rightarrow H_2 + CH_3CHCH_3$	7.49	7.68 [b]
C4	H-R5	$H + CH_3(CH_2)_2CH_3 \rightarrow H_2 + CH_2(CH_2)_2CH_3$	10.05	10.07 [c]
	H-R6	$H + CH_3(CH_2)_2CH_3 \rightarrow H_2 + CH_3CHCH_2CH_3$	7.39	7.21 [c]
C10	H-R26	$H + CH_3(CH_2)_8CH_3 \rightarrow H_2 + CH_2(CH_2)_8CH_3$	9.82	10.1 [d]
	H-R27	$H + CH_3(CH_2)_8CH_3 \rightarrow H_2 + CH_3CH(CH_2)_7CH_3$	7.15	7.2 [d]
	H-R28	$H + CH_3(CH_2)_8CH_3 \rightarrow H_2 + CH_3CH_2CH(CH_2)_6CH_3$	7.05	7.1 [d]
	H-R29	$H + CH_3(CH_2)_8CH_3 \rightarrow H_2 + CH_3(CH_2)_2CH(CH_2)_5CH_3$	7.04	7.0 [d]
	H-R30	$H + CH_3(CH_2)_8CH_3 \rightarrow H_2 + CH_3(CH_2)_3CH(CH_2)_4CH_3$	7.02	7.0 [d]
C18	H-R82	$H + CH_3(CH_2)_{16}CH_3 \rightarrow H_2 + CH_2(CH_2)_{16}CH_3$	9.84	10.85 [e]
	H-R83	$H + CH_3(CH_2)_{16}CH_3 \rightarrow H_2 + CH_3CH(CH_2)_{15}CH_3$	7.21	7.82 [e]
		H-R84 ~ H-R90	6.91~7.10	7.7~7.8 [e]

[a] Espinosa-Garcia [52] at the CCSD(T)/cc-pVTZ//MP2(full)/6-31G(d,p) level. [b] Sivaramakrishnan et al. [49] at the CCSD(T)/aug-cc-pV∞Z//MP2/6-311++G(d,p) level. [c] Peukert et al. [47] at the CCSD(T)/cc-pV∞Z//M06-2X/cc-pVTZ level. [d] Wang et al. [72] at the CBS-QB3//M06-2X/6-311++G(d,p) level. [e] Chi and You [73] at the M06-2X/6-311++G(d,p) level.

For the reaction systems of *n*-C_nH_{2n+2} + OH, Gruber and Czako [74] calculated the reactions of CH_4 and C_2H_6 with OH at the CCSD(T)-F12b/aug-cc-pVnZ//CCSD(T)-F12b/aug-cc-pVTZ level. Khaled et al. [48] studied the reaction of C_2H_6 with OH at the CCSD(T)/cc-pV(T,Q)Z//MP2/cc-pVTZ level. Despite employing these very high-level methods, the differences in results were generally less than 0.4 kcal/mol when compared with the ONIOM method. Sivaramakrishnan et al. [42,50] studied the reactions of *n*-C_3H_8, *n*-C_4H_{10}, and *n*-C_5H_{12} with OH at the G3//B3LYP level. The ONIOM method aligns precisely with the G3//B3LYP results for the hydrogen abstraction reaction from the CH_3 group, except OH-R5, where the difference is 0.83 kcal/mol. However, it is important to note

that the results using the ONIOM method for the hydrogen abstraction reactions from the CH_2 groups differ significantly from those obtained using the G3//B3LYP method, as indicated in Table 9. This discrepancy may be attributed to the G3//B3LYP method's tendency to predict tighter transition state structures, resulting in higher energy barriers. Furthermore, Seal et al. [75] studied the hydrogen abstraction reactions of 1-butanol, labeled as $H_3C^{(1)}$–$H_2C^{(2)}$–$H_2C^{(3)}$–$H_2C^{(4)}$-OH, by OH radical at the CCSD(T)/F12a/jun-cc-pVTZ//M08-HX/MG3S level. Their results show EBs of 0.39 kcal/mol (1.98 kcal/mol for OH-R7), −0.82 kcal/mol (−0.27 kcal/mol for OH-R8), −0.50 kcal/mol (−0.13 kcal/mol for OH-R9), and −0.27 kcal/mol for the reactions occurring from C1 to C4. In comparison, the EB values obtained using the ONIOM method are consistent and reliable. The differences in these results can be attributed to variations in the geometry optimization methods.

Table 9. The calculated EBs for the hydrogen abstraction reactions of *n*-C_nH_{2n+2} + OH (*n* = 1–5) (unit: kcal/mol).

	No.	Reactions	ONIOM	Reference
C1	OH-R1	$OH + CH_4 \rightarrow H_2O + CH_3$	5.02	4.78 [a]
C2	OH-R2	$OH + CH_3CH_3 \rightarrow H_2O + CH_2CH_3$	2.63	2.18 [a], 2.22 [b]
C3	OH-R3	$OH + CH_3CH_2CH_3 \rightarrow H_2O + CH_2CH_2CH_3$	1.81	1.93 [c]
	OH-R4	$OH + CH_3CH_2CH_3 \rightarrow H_2O + CH_3CHCH_3$	0.49	0.93 [c]
C4	OH-R5	$OH + CH_3(CH_2)_2CH_3 \rightarrow H_2O + CH_2(CH_2)_2CH_3$	2.89	2.06 [c]
	OH-R6	$OH + CH_3(CH_2)_2CH_3 \rightarrow H_2O + CH_3CHCH_2CH_3$	0.99	0.72 [c]
C5	OH-R7	$OH + CH_3(CH_2)_3CH_3 \rightarrow H_2O + CH_2(CH_2)_3CH_3$	1.98	1.98 [d]
	OH-R8	$OH + CH_3(CH_2)_3CH_3 \rightarrow H_2O + CH_3CH(CH_2)_2CH_3$	−0.27	0.84 [d]
	OH-R9	$OH + CH_3(CH_2)_3CH_3 \rightarrow H_2O + CH_3CH_2CHCH_2CH_3$	−0.13	0.40 [d]

[a] Gruber and Czakó [74] at the CCSD(T)-F12b/aug-cc-pVnZ//CCSD(T)-F12b/aug-cc-pVTZ. [b] Khaled et al. [48] at the CCSD(T)/cc-pV(T,Q)Z//MP2/cc-pVTZ. [c] Sivaramakrishnan et al. [50] at the G3//B3LYP level. [d] Sivaramakrishnan and Michael [42] at the G3//B3LYP level.

For the reaction systems of *n*-C_nH_{2n+2} + HO_2, Aguilera et al. [37] provided accurate benchmark data for hydrogen abstraction reactions of *n*-C_nH_{2n+2} + HO_2 (*n* = 2–4) at the CCSD(T)/cc-pVTZ//B3LYP/def2-TZVP level. More recently, Hashemi et al. [44] investigated the reactions of propane with HO_2 at the CCSD(T)/cc-pV(T,Q)Z level, finding the difference in results compared to the ONIOM method to be less than 0.30 kcal/mol These data were compared with the results using the ONIOM method, as detailed in Table 10. It is noteworthy that the discrepancies in EBs for hydrogen abstraction reactions occurring at the CH_3 groups are generally less than 0.4 kcal/mol. However, notable exceptions are observed in reactions occurring at the CH_2 groups in HO_2-R4 and HO_2-R6, where the differences in EBs are 0.77 kcal/mol and 0.98 kcal/mol, respectively.

Table 10. The calculated EBs for the hydrogen abstraction reactions of *n*-C_nH_{2n+2} + HO_2 (*n* = 1–4) (unit: kcal/mol).

	No.	Reactions	ONIOM	Reference
C1	HO_2-R1	$HO_2 + CH_4 \rightarrow H_2O_2 + CH_3$	24.11	24.00 [a]
C2	HO_2-R2	$HO_2 + CH_3CH_3 \rightarrow H_2O_2 + CH_2CH_3$	19.90	19.50 [a]
C3	HO_2-R3	$HO_2 + CH_3CH_2CH_3 \rightarrow H_2O_2 + CH_2CH_2CH_3$	19.40	19.60 [a], 19.30 [b]
	HO_2-R4	$HO_2 + CH_3CH_2CH_3 \rightarrow H_2O_2 + CH_3CHCH_3$	16.86	16.09 [a], 16.60 [b]
C4	HO_2-R5	$HO_2 + CH_3(CH_2)_2CH_3 \rightarrow H_2O_2 + CH_2(CH_2)_2CH_3$	19.31	19.46 [a]
	HO_2-R6	$HO_2 + CH_3(CH_2)_2CH_3 \rightarrow H_2O_2 + CH_3CHCH_2CH_3$	16.37	15.39 [a]

[a] Aquilera et al. [37] at the CCSD(T)/cc-pVTZ//B3LYP/def2-TZVP level with optimization by scaling factor of 1.053. [b] Hashemi et al. [44] at the CCSD(T)/cc-pV(T,Q)Z level.

3.4.3. Comparison with Saturated Methyl Ester

Zhang and Zhang [32] and Chi and You [73] conducted studies on the reactions of $C_{15}H_{31}COOCH_3$ + H, employing the ONIOM[QCISD(T)/CBS:DFT] and GEBF[CCSD(T)-

F12a/cc-pVTZ] methods, respectively. The present study compared similar reactions involving $C_{15}H_{31}COOCH_3$ + H and *n*-$C_{16}H_{34}$ + H. This comparison is pertinent as the two molecules have very similar structures, as depicted in Figure 8. As observed in Figure 8, the predicted EBs for the reaction involving $C_{15}H_{31}COOCH_3$ + H are generally close across all reaction sites, with notable exceptions at two reaction sites, No. 12 and No. 14. Here, the differences are 0.59 kcal/mol and 1.01 kcal/mol compared to Zhang and Zhang [32], and 1.19 kcal/mol and 0.98 kcal/mol when compared to Chi and You [73].

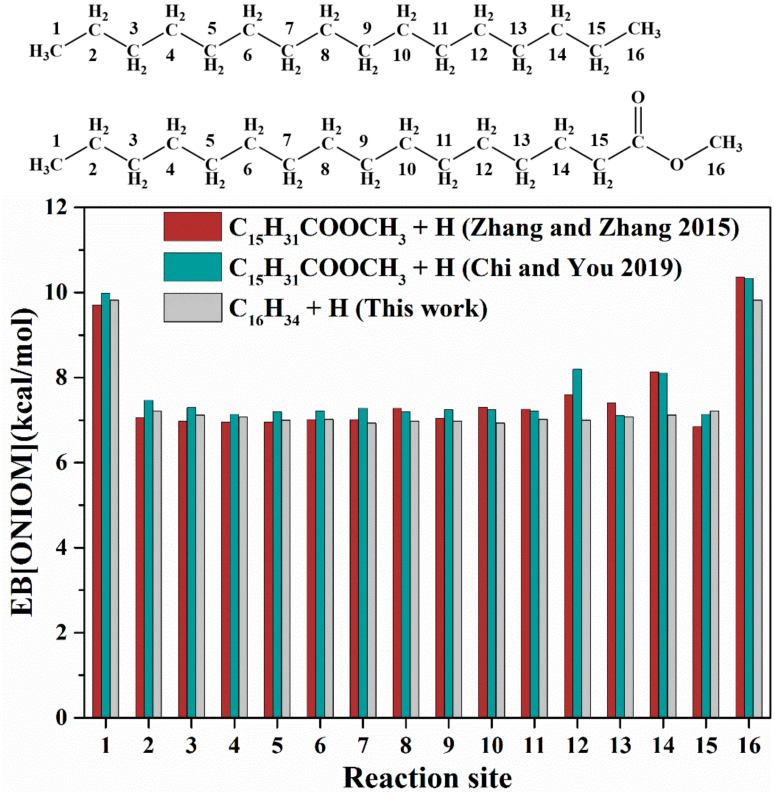

Figure 8. The EBs for the hydrogen abstraction reactions of $C_{15}H_{31}COOCH_3$ + H and *n*-$C_{16}H_{34}$ + H [32,73].

As expected, there is a notable agreement in the EBs at the reaction sites sufficiently distant from the ester group (specifically, Nos. 1–11 as illustrated in Figure 8), with differences generally being less than 0.3 kcal/mol. This can be understood by the fact that the influence of the ester group on the reaction decreases with moving away from its CAP and becomes non-negligible at the site of No. 12. The biggest difference between the two reactions occurs at the reaction occurring at the reaction site of No. 14, up to 1.0 kcal/mol. This indicates that the hydrogen abstraction from the No. 14 site is strongly affected by the ester functional group.

3.4.4. Comparison to Unsaturated Methyl Ester

Zhang et al. [34] also employed the ONIOM[QCISD(T)/CBS:DFT] method to study the hydrogen abstraction reactions between unsaturated methyl esters and hydrogen atoms. The calculated EBs for the hydrogen abstraction reactions of $C_{17}H_{33}COOCH_3$ and *n*-$C_{18}H_{38}$ are compared, as shown in Figure 9. It is observed that the EBs for $C_{17}H_{33}COOCH_3$ + H and *n*-$C_{18}H_{38}$ + H at the reaction sites of Nos. 1–6 generally differ by no more than 0.4 kcal/mol. However, the differences significantly increase with the reactions occurring at the reaction sites (Nos. 8–11) near the C=C double bond, with the largest difference being approximately 4.60 kcal/mol at the reaction site of No. 9 and No. 10. The differences in EBs reduce to 2.12 kcal/mol at the site of No. 8 and 2.24 kcal/mol at the site of No. 11, while the differences at the reaction sites of No. 7 and No. 12 are 0.51 kcal/mol and 0.78 kcal/mol,

respectively. When the reaction occurs at a site more than three -CH_2 groups away from the C=C double bond, the general differences in EBs are reduced to less than 0.40 kcal/mol.

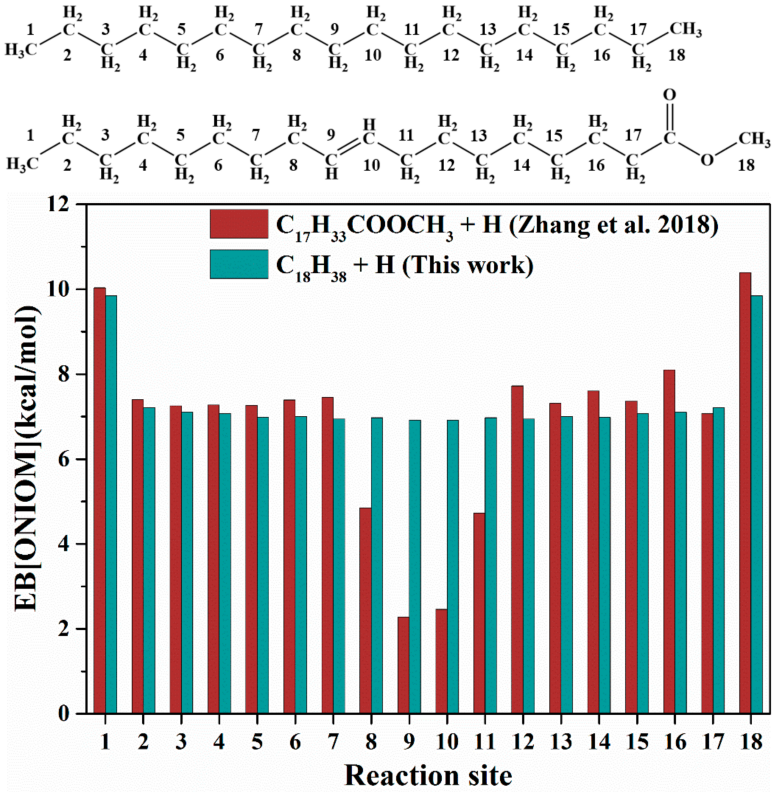

Figure 9. The EBs for the hydrogen abstraction reactions of $C_{17}H_{33}COOCH_3$ + H and *n*-$C_{18}H_{38}$ + H [32].

The agreement in EBs at the reaction sites, which are more than two carbon atoms away from the ester group, is generally satisfactory and remains below 0.60 kcal/mol. The maximum difference observed is 1.00 kcal/mol for the reaction occurring at site of No. 16. Consequently, it can be concluded that the ester group exerts a similar effect in both saturated and unsaturated esters. In addition, the influence of ester group on the hydrogen abstraction reactions of larger molecules by hydrogen atoms is weaker compared to that of the C=C double bond.

4. Conclusions

An ONIOM[QCISD(T)/CBS:DFT] method was proposed and systematically validated in the present study for the hydrogen abstraction of straight-chain alkanes, *n*-C_nH_{2n+2} (n = 1–16), by H, OH, and HO_2 radicals. Two QCISD(T)/CBS methods were used to validate the ONIOM method. The comparison with the previous studies of large biodiesel molecules further substantiated the computational accuracy of the ONIOM method. Some important conclusions can be drawn from the work.

First, the computational uncertainty between the two QCISD(T)/CBS methods is typically less than 0.20 kcal/mol. It again proved that the $[QCISD(T)/CBS]_2$ method through extrapolation from cc-pVDZ, cc-pVTZ to CBS with a second-order Møller–Plesset perturbation theory correction (MP2) is as accurate as the $[QCISD(T)/CBS]_1$ method.

Second, the chemically active portion CAP (2,2) is minimally and reasonably required for the present reaction system. This is because it can predict the EB and ΔH for the studied reactions with satisfactory accuracy. The differences, when compared to the $[QCISD(T)/CBS]_2$ method, are generally less than 0.10 kcal/mol.

Third, a comparison with the thermochemical data (EB) from kinetic modeling reveals that EBs are typically considered constants. This is because the hydrogen abstraction reactions of *n*-alkanes can be categorized into two types: reactions occurring at primary

sites (CH_3 groups) and reactions at other sites (CH_2 groups). The present results indicate that this classification is reasonable for the reactions of *n*-C_nH_{2n+2} + H (or HO_2). However, it is not suitable for the reactions of *n*-C_nH_{2n+2} + OH, owing to the significant variation in EBs, particularly for the reactions occurring at the CH_2 groups.

Finally, by comparing large straight-chain alkanes, specifically *n*-$C_{16}H_{34}$ and *n*-$C_{18}H_{38}$, with large methyl ester molecules, such as $C_{15}H_{31}COOCH_3$ and $C_{17}H_{33}COOCH_3$, we observed that the influence of functional groups (the ester group and C=C double bond) becomes negligible at the reaction site when it is more than two nonhydrogen atoms away from the functional group. At these distances, the thermochemistry of the methyl ester molecules closely resembles that of straight-chain alkanes. Furthermore, it is noted that the C=C double bond exerts a greater influence on neighboring atoms than the ester group in hydrogen abstraction reactions by hydrogen atoms.

Overall, this study presents a practically useful theoretical methodology, along with comprehensive thermochemical data, for the hydrogen abstraction reactions of *n*-C_nH_{2n+2} (*n* = 1–16), by H, OH, and HO2 radicals. These data are valuable for the chemical kinetics calculation involving large straight-chain alkanes.

Supplementary Materials: The following supporting information can be downloaded at: https://www.mdpi.com/article/10.3390/sym16030367/s1, Cartesian coordinates of optimized geometries for all species and the calculated results (EB and ΔH) for the hydrogen abstraction reactions of *n*-C_nH_{2n+2} + H (*n* = 10–16), *n*-C_nH_{2n+2} + OH (*n* = 9–16), and *n*-C_nH_{2n+2} + HO_2 (*n* = 8–16) using the ONIOM method. The figures of IRC curves, using H-R66 and H-R72 as examples. Figure S1: The IRC curves of the reactions (a) H-R66: H + $CH_3(CH_2)_{14}CH3 \rightarrow H_2 + CH_3CH(CH_2)_{13}CH_3$ and (b) H-R72: H + $CH_3(CH_2)_{14}CH_3 \rightarrow H_2 + CH_3(CH_2)_6CH(CH_2)_7CH_3$; Table S1: The calculated results (EB and ΔH) for the hydrogen abstraction reactions of *n*-C_nH_{2n+2} + H (*n* = 10–16) using the ONIOM method; Table S2: The calculated results (EB and ΔH) for the hydrogen abstraction reactions of *n*-C_nH_{2n+2} + OH (*n* = 9–16) using the ONIOM method; Table S3: The calculated results (EB and ΔH) for the hydrogen abstraction reactions of *n*-C_nH_{2n+2} + HO_2 (*n* = 8–16) using the ONIOM method.

Author Contributions: Conceptualization, P.Z. and L.Z.; methodology, Y.C. and Q.M.; software, Y.C.; validation, Y.C. and Q.M.; formal analysis, Y.C.; investigation, Y.C.; resources, H.P.; data curation, Y.C.; writing—original draft preparation, Y.C.; writing—review and editing, P.Z. and H.P.; visualization, Y.C.; supervision, P.Z.; project administration, P.Z.; funding acquisition, H.P. All authors have read and agreed to the published version of the manuscript.

Funding: This work is financially supported by the National Natural Science Foundation of China (No. 52176134) and partially by the APRC-CityU New Research Initiatives/Infrastructure Support from Central of City University of Hong Kong (No. 9610601).

Data Availability Statement: The dataset used and/or analyzed during the current study is available from the corresponding author.

Acknowledgments: The authors would like to thank the reviewers for their valuable comments and the administrative staff.

Conflicts of Interest: The authors declare no conflicts of interest.

Nomenclature

CAP	Chemically active portion
CBS	Complete basis set
CCSD(T)	Coupled cluster with single, double, and perturbative triple excitations
DFT	Density functional theory
DZ	Double Zeta (referring to the quality of a basis set)
EB	Energy barrier
ΔH	Heat of reaction
IRC	Intrinsic reaction coordinate
MP2	Second-order Møller–Plesset perturbation theory correction
ONIOM	Our own n-layered integrated molecular orbital and molecular mechanics

pV	Polarized valence (referring to the type of functions in a basis set)
QCISD(T)	Quadratic configuration interaction with single and double excitations and a perturbative estimate of triple excitations
QZ	Quadruple Zeta (referring to the quality of a basis set)
TZ	Triple Zeta (referring to the quality of a basis set)
ZPE	Zero-point energy
cc	Correlation-consistent (referring to the type of basis set)

References

1. Westbrook, C.K.; Dryer, F.L. Chemical kinetics and modeling of combustion processes. *Symp. Int. Combust.* **1981**, *18*, 749–767. [CrossRef]
2. Dagaut, P.; Cathonnet, M. The ignition, oxidation, and combustion of kerosene: A review of experimental and kinetic modeling. *Prog. Energy Combust. Sci.* **2006**, *32*, 48–92. [CrossRef]
3. Edwards, T.; Colket, M.; Cernansky, N.; Dryer, F.; Egolfopoulos, F.; Friend, D.; Law, E.; Lenhert, D.; Lindstedt, P.; Pitsch, H.; et al. Development of an Experimental Database and Kinetic Models for Surrogate Jet Fuels. In Proceedings of the 45th AIAA Aerospace Sciences Meeting and Exhibit, AIAA-2007-0770, Reno, NV, USA, 8–11 January 2007.
4. Farrell, J.T.; Cernansky, N.P.; Dryer, F.L.; Law, C.K.; Friend, D.G.; Hergart, C.A.; McDavid, R.M.; Patel, A.K.; Mueller, C.J.; Pitsch, H. *Development of an Experimental Database and Kinetic Models for Surrogate Diesel Fuels*; SAE Technical Paper 2007-01-0201; SAE: Warrendale, PA, USA, 2007. [CrossRef]
5. Pitz, W.J.; Cernansky, N.P.; Dryer, F.L.; Egolfopoulos, F.N.; Farrell, J.T.; Friend, D.G.; Pitsch, H. *Development of an Experimental Database and Chemical Kinetic Models for Surrogate Gasoline Fuels*; SAE Technical Paper 2007-01-0175; SAE: Warrendale, PA, USA, 2007.
6. Pitz, W.J.; Mueller, C.J. Recent progress in the development of diesel surrogate fuels. *Prog. Energy Combust. Sci.* **2011**, *37*, 330–350. [CrossRef]
7. Sarathy, S.; Farooq, A.; Kalghatgi, G.T. Recent progress in gasoline surrogate fuels. *Prog. Energy Combust. Sci.* **2018**, *65*, 67–108. [CrossRef]
8. Mehl, M.; Pitz, W.J.; Westbrook, C.K.; Curran, H. Kinetic modeling of gasoline surrogate components and mixtures under engine conditions. *Proc. Combust. Inst.* **2011**, *33*, 193–200. [CrossRef]
9. Jerzembeck, S.; Peters, N.; Pepiotdesjardins, P.; Pitsch, H. Laminar burning velocities at high pressure for primary reference fuels and gasoline: Experimental and numerical investigation. *Combust. Flame* **2009**, *156*, 292–301. [CrossRef]
10. Sileghem, L.; Alekseev, V.; Vancoillie, J.; Van Geem, K.; Nilsson, E.; Verhelst, S.; Konnov, A. Laminar burning velocity of gasoline and the gasoline surrogate components iso-octane, n-heptane and toluene. *Fuel* **2013**, *112*, 355–365. [CrossRef]
11. Lemaire, R.; Faccinetto, A.; Therssen, E.; Ziskind, M.; Focsa, C.; Desgroux, P. Experimental comparison of soot formation in turbulent flames of Diesel and surrogate Diesel fuels. *Proc. Combust. Inst.* **2009**, *32*, 737–744. [CrossRef]
12. Mati, K.; Ristori, A.; Gaïl, S.; Pengloan, G.; Dagaut, P. The oxidation of a diesel fuel at 1–10 atm: Experimental study in a JSR and detailed chemical kinetic modeling. *Proc. Combust. Inst.* **2007**, *31*, 2939–2946. [CrossRef]
13. Honnet, S.; Seshadri, K.; Niemann, U.; Peters, N. A surrogate fuel for kerosene. *Proc. Combust. Inst.* **2009**, *32*, 485–492. [CrossRef]
14. Dagaut, P.; El Bakali, A.; Ristori, A. The combustion of kerosene: Experimental results and kinetic modelling using 1- to 3-component surrogate model fuels. *Fuel* **2006**, *85*, 944–956. [CrossRef]
15. Strelkova, M.I.; Kirillov, I.A.; Potapkin, B.V.; Safonov, A.A.; Sukhanov, L.P.; Umanskiy, S.Y.; Deminsky, M.A.; Dean, A.J.; Varatharajan, B.; Tentner, A.M. Detailed and reduced mechanisms of jet a combustion at high temperatures. *Combust. Sci. Technol.* **2008**, *180*, 1788–1802. [CrossRef]
16. Mawid, M.; Sekar, B. Development of a detailed JP-8/Jet-A chemical kinetic mechanism for high pressure conditions in gas turbine combustors. In Proceedings of the ASME Turbo Expo 2006: Power for Land, Sea, and Air, Barcelona, Spain, 8–11 May 2006; pp. 369–388.
17. Dahm, K.; Virk, P.; Bounaceur, R.; Battin-Leclerc, F.; Marquaire, P.; Fournet, R.; Daniau, E.; Bouchez, M. Experimental and modelling investigation of the thermal decomposition of n-dodecane. *J. Anal. Appl. Pyrolysis* **2004**, *71*, 865–881. [CrossRef]
18. Westbrook, C.K.; Dryer, F.L. Chemical kinetic modeling of hydrocarbon combustion. *Prog. Energy Combust. Sci.* **1984**, *10*, 1–57. [CrossRef]
19. Simmie, J.M. Detailed chemical kinetic models for the combustion of hydrocarbon fuels. *Prog. Energy Combust. Sci.* **2003**, *29*, 599–634. [CrossRef]
20. Ranzi, E.; Frassoldati, A.; Grana, R.; Cuoci, A.; Faravelli, T.; Kelley, A.P.; Law, C.K. Hierarchical and comparative kinetic modeling of laminar flame speeds of hydrocarbon and oxygenated fuels. *Prog. Energy Combust. Sci.* **2012**, *38*, 468–501. [CrossRef]
21. Curran, H.; Gaffuri, P.; Pitz, W.; Westbrook, C. A Comprehensive modeling study of n-heptane oxidation. *Combust. Flame* **1998**, *114*, 149–177. [CrossRef]
22. Curran, H.; Gaffuri, P.; Pitz, W.; Westbrook, C. A comprehensive modeling study of iso-octane oxidation. *Combust. Flame* **2002**, *129*, 253–280. [CrossRef]
23. Westbrook, C.K.; Pitz, W.J.; Herbinet, O.; Curran, H.J.; Silke, E.J. A comprehensive detailed chemical kinetic reaction mechanism for combustion of n-alkane hydrocarbons from n-octane to n-hexadecane. *Combust. Flame* **2009**, *156*, 181–199. [CrossRef]

24. Ritter, E.R.; Bozzelli, J.W. THERM: Thermodynamic property estimation for gas phase radicals and molecules. *Int. J. Chem. Kinet.* **1991**, *23*, 767–778. [CrossRef]
25. Lay, T.H.; Bozzelli, J.W.; Dean, A.M.; Ritter, E.R. Hydrogen atom bond increments for calculation of thermodynamic properties of hydrocarbon radical species. *J. Phys. Chem.* **1995**, *99*, 14514–14527. [CrossRef]
26. Benson, S.W. *Thermochemical Kinetics*; Wiley: Hoboken, NJ, USA, 1976.
27. Papajak, E.; Truhlar, D.G. What are the most efficient basis set strategies for correlated wave function calculations of reaction energies and barrier heights? *J. Chem. Phys.* **2012**, *137*, 064110. [CrossRef] [PubMed]
28. Zádor, J.; Taatjes, C.A.; Fernandes, R.X. Kinetics of elementary reactions in low-temperature autoignition chemistry. *Prog. Energy Combust. Sci.* **2011**, *37*, 371–421. [CrossRef]
29. Goldsmith, C.F.; Magoon, G.R.; Green, W.H. Database of Small Molecule Thermochemistry for Combustion. *J. Phys. Chem. A* **2012**, *116*, 9033–9057. [CrossRef] [PubMed]
30. El-Nahas, A.M.; Navarro, M.V.; Simmie, J.M.; Bozzelli, J.W.; Curran, H.J.; Dooley, S.; Metcalfe, W. Enthalpies of formation, bond dissociation energies and reaction paths for the decomposition of model biofuels: Ethyl propanoate and methyl butanoate. *J. Phys. Chem. A* **2007**, *111*, 3727–3739. [CrossRef]
31. Osmont, A.; Catoire, L.; Dagaut, P. Thermodynamic data for the modeling of the thermal decomposition of biodiesel. 1. Saturated and monounsaturated FAMEs. *J. Phys. Chem. A* **2009**, *114*, 3788–3795. [CrossRef] [PubMed]
32. Zhang, L.; Zhang, P. Towards high-level theoretical studies of large biodiesel molecules: An ONIOM [QCISD(T)/CBS:DFT] study of hydrogen abstraction reactions of $C_nH_{2n+1}COOC_mH_{2m+1}$ + H. *Phys. Chem. Chem. Phys.* **2015**, *17*, 200–208. [CrossRef]
33. Vreven, T.; Byun, K.S.; Komáromi, I.; Dapprich, S.; Montgomery, J.A., Jr.; Morokuma, K.; Frisch, M.J. Combining quantum mechanics methods with molecular mechanics methods in ONIOM. *J. Chem. Theory Comput.* **2006**, *2*, 815–826. [CrossRef]
34. Zhang, L.; Meng, Q.; Chi, Y.; Zhang, P. Toward high-level theoretical studies of large biodiesel molecules: An ONIOM [QCISD(T)/CBS:DFT] study of the reactions between unsaturated methyl esters ($C_nH_{2n-1}COOCH_3$) and hydrogen radical. *J. Phys. Chem. A* **2018**, *122*, 4882–4893. [CrossRef]
35. He, C.; Chi, Y.; Zhang, P. Approximate reconstruction of torsional potential energy surface based on voronoi tessellation. *Proc. Combust. Inst.* **2020**, *38*, 757–766. [CrossRef]
36. Meng, Q.; Zhang, L.; Chen, Q.; Chi, Y.; Zhang, P. Influence of torsional anharmonicity on the reactions of methyl butanoate with hydroperoxyl radical. *J. Phys. Chem. A* **2020**, *124*, 8643–8652. [CrossRef] [PubMed]
37. Aguilera-Iparraguirre, J.; Curran, H.J.; Klopper, W.; Simmie, J.M. Accurate benchmark calculation of the reaction barrier height for hydrogen abstraction by the hydroperoxyl radical from methane. implications for C_nH_{2n+2} where $n = 2 \rightarrow 4$. *J. Phys. Chem. A* **2008**, *112*, 7047–7054. [CrossRef] [PubMed]
38. Cohen, N. Are reaction rate coefficients additive? Revised transition state theory calculations for OH + alkane reactions. *Int. J. Chem. Kinet.* **1991**, *23*, 397–417. [CrossRef]
39. Cohen, N. The use of transition-state theory to extrapolate rate coefficients for reactions of H atoms with alkanes. *Int. J. Chem. Kinet.* **1991**, *23*, 683–700. [CrossRef]
40. Liu, D.; Khaled, F.; Giri, B.R.; Assaf, E.; Fittschen, C.; Farooq, A. H-abstraction by OH from large branched alkanes: Overall rate measurements and site-specific tertiary rate calculations. *J. Phys. Chem. A* **2017**, *121*, 927–937. [CrossRef] [PubMed]
41. Badra, J.; Elwardany, A.; Farooq, A. Shock tube measurements of the rate constants for seven large alkanes + OH. *Proc. Combust. Inst.* **2015**, *35*, 189–196. [CrossRef]
42. Sivaramakrishnan, R.; Michael, J.V. Rate constants for OH with selected large alkanes: Shock-tube measurements and an improved group scheme. *J. Phys. Chem. A* **2009**, *113*, 5047–5060. [CrossRef]
43. Hashemi, H.; Christensen, J.M.; Glarborg, P.; Gersen, S.; Essen, M.; Wand, Z.; Ju, Y. High-pressure oxidation of n-butane. *Int. J. Chem. Kinet.* **2023**, *55*, 688–706. [CrossRef]
44. Hashemi, H.; Christensen, J.M.; Harding, L.B.; Klippenstein, S.J.; Glarborg, P. High-pressure oxidation of propane. *Proc. Combust. Inst.* **2018**, *37*, 461–468. [CrossRef]
45. Hashemi, H.; Jacobsen, J.G.; Rasmussen, C.T.; Christensen, J.M.; Glarborg, P.; Gersen, S.; van Essen, M.; Levinsky, H.B.; Klippenstein, S.J. High-pressure oxidation of ethane. *Combust. Flame* **2017**, *182*, 150–166. [CrossRef]
46. Hashemi, H.; Christensen, J.M.; Gersen, S.; Levinsky, H.; Klippenstein, S.J.; Glarborg, P. High-pressure oxidation of methane. *Combust. Flame* **2016**, *172*, 349–364. [CrossRef]
47. Peukert, S.L.; Sivaramakrishnan, R.; Michael, J.V. High temperature rate constants for H/D+ n-C_4H_{10} and i-C_4H_{10}. *Proc. Combust. Inst.* **2015**, *35*, 171–179. [CrossRef]
48. Khaled, F.; Giri, B.R.; Szőri, M.; Viskolcz, B.; Farooq, A. An experimental and theoretical study on the kinetic isotope effect of C2H6 and C2D6 reaction with OH. *Chem. Phys. Lett.* **2015**, *641*, 158–162. [CrossRef]
49. Sivaramakrishnan, R.; Michael, J.; Ruscict, B. High-temperature rate constants for H/D+ C_2H_6 and C_3H_8. *Int. J. Chem. Kinet.* **2012**, *44*, 194–205. [CrossRef]
50. Sivaramakrishnan, R.; Srinivasan, N.; Su, M.-C.; Michael, J. High temperature rate constants for OH+ alkanes. *Proc. Combust. Inst.* **2009**, *32*, 107–114. [CrossRef]
51. Krasnoperov, L.N.; Michael, J. Shock tube studies using a novel multipass absorption cell: Rate constant results for OH + H2 and OH + C2H6. *J. Phys. Chem. A* **2004**, *108*, 5643–5648. [CrossRef]

52. Espinosa-Garcia, J. New analytical potential energy surface for the CH4+H hydrogen abstraction reaction: Thermal rate constants and kinetic isotope effects. *J. Chem. Phys.* **2002**, *116*, 10664–10673. [CrossRef]
53. Wu, J.; Ning, H.; Xu, X.; Ren, W. Accurate entropy calculation for large flexible hydrocarbons using a multi-structural 2-dimensional torsion method. *Phys. Chem. Chem. Phys.* **2019**, *21*, 10003–10010. [CrossRef]
54. Chi, Y.; Meng, Q.; He, C.; Zhang, P. Metric-based assessment method for MS-T formalism with small subsets of torsional conformers. *J. Phys. Chem. A* **2022**, *126*, 8305–8314. [CrossRef]
55. Meng, Q.; Lin, X.; Zhai, Y.; Zhang, L.; Zhang, P.; Sheng, L. A theoretical investigation on Bell-Evans-Polanyi correlations for hydrogen abstraction reactions of large biodiesel molecules by H and OH radicals. *Combust. Flame* **2020**, *214*, 394–406. [CrossRef]
56. Sarathy, S.M.; Thomson, M.J.; Pitz, W.J.; Lu, T. An experimental and kinetic modeling study of methyl decanoate combustion. *Proc. Combust. Inst.* **2011**, *33*, 399–405. [CrossRef]
57. Becke, A.D. Density-functional thermochemistry. III. The role of exact exchange. *J. Chem. Phys.* **1993**, *98*, 5648–5652. [CrossRef]
58. Zhao, Y.; Truhlar, D.G. A new local density functional for main-group thermochemistry, transition metal bonding, thermochemical kinetics, and noncovalent interactions. *J. Chem. Phys.* **2006**, *125*, 194101. [CrossRef] [PubMed]
59. Dunning, T.H., Jr. Gaussian basis sets for use in correlated molecular calculations. I. The atoms boron through neon and hydrogen. *J. Chem. Phys.* **1989**, *90*, 1007–1023. [CrossRef]
60. Kendall, R.A.; Dunning, T.H., Jr.; Harrison, R.J. Electron affinities of the first-row atoms revisited. Systematic basis sets and wave functions. *J. Chem. Phys.* **1992**, *96*, 6796–6806. [CrossRef]
61. Martin, J.M.; Uzan, O. Basis set convergence in second-row compounds. The importance of core polarization functions. *Chem. Phys. Lett.* **1998**, *282*, 16–24. [CrossRef]
62. Zhang, P.; Klippenstein, S.J.; Law, C.K. Ab initio kinetics for the decomposition of hydroxybutyl and butoxy radicals of *n*-butanol. *J. Phys. Chem. A* **2013**, *117*, 1890–1906. [CrossRef]
63. Meng, Q.; Chi, Y.; Zhang, L.; Zhang, P.; Sheng, L. Towards high-level theoretical studies of large biodiesel molecules: An ONIOM/RRKM/Master-equation approach to the isomerization and dissociation kinetics of methyl decanoate radicals. *Phys. Chem. Chem. Phys.* **2019**, *21*, 5232–5242. [CrossRef]
64. Frisch, M.J.; Trucks, G.W.; Schlegel, H.B.; Scuseria, G.E.; Robb, M.A.; Cheeseman, J.R.; Scalmani, G.; Barone, V.; Mennucci, B.; Petersson, G.A.; et al. *Gaussian 09*; Revision A.02; Gaussian, Inc.: Wallingford, CT, USA, 2009.
65. Battin-Leclerc, F.; Blurock, E.; Bounaceur, R.; Fournet, R.; Glaude, P.-A.; Herbinet, O.; Sirjean, B.; Warth, V. Towards cleaner combustion engines through groundbreaking detailed chemical kinetic models. *Chem. Soc. Rev.* **2011**, *40*, 4762–4782. [CrossRef]
66. Nehse, M.; Warnat, J.; Chevalier, C. Kinetic modeling of the oxidation of large aliphatic hydrocarbons. *Symp. Int. Combust.* **1996**, *26*, 773–780. [CrossRef]
67. Petrova, M.; Williams, F. A small detailed chemical-kinetic mechanism for hydrocarbon combustion. *Combust. Flame* **2006**, *144*, 526–544. [CrossRef]
68. Warnatz, J. Resolution of gas phase and surface combustion chemistry into elementary reactions. *Symp. Int. Combust.* **1992**, *24*, 553–579. [CrossRef]
69. Cohen, N. The use of transition-state theory to extrapolate rate coefficients for reactions of oh with alkanes. *Int. J. Chem. Kinet.* **1982**, *14*, 1339–1362. [CrossRef]
70. Evans, M.G.; Polanyi, M. Inertia and driving force of chemical reactions. *Trans. Faraday Soc.* **1938**, *34*, 11–24. [CrossRef]
71. Rossi, I.; Truhlar, D.G. Improved general scaling factors and systematic tests of the SAC method for estimating correlation energies of molecules. *Chem. Phys. Lett.* **1995**, *234*, 64–70. [CrossRef]
72. Wang, P.; Yan, J.; Yan, T.; Ao, C.; Zhang, L.; Lei, L. Kinetic study of H-abstraction and preliminary pyrolysis of n-decane in post-injection fuels. *Combust. Flame* **2024**, *262*, 113367. [CrossRef]
73. Chi, Y.; You, X. Kinetics of hydrogen abstraction reactions of methyl palmitate and octadecane by hydrogen atoms. *J. Phys. Chem. A* **2019**, *123*, 3058–3067. [CrossRef]
74. Gruber, B.; Czakó, G. Benchmark ab initio characterization of the abstraction and substitution pathways of the OH+ CH_4/C_2H_6 reactions. *Phys. Chem. Chem. Phys.* **2020**, *22*, 14560–14569. [CrossRef]
75. Seal, P.; Oyedepo, G.; Truhlar, D.G. Kinetics of the hydrogen atom abstraction reactions from 1-butanol by hydroxyl radical: Theory matches experiment and more. *J. Phys. Chem. A* **2013**, *117*, 275–282. [CrossRef]